Linthotage Dushantha Lochana Perera
Wijerupage Sardha Wijesoma
Martin David Adams

Centre for Intelligent Machines (Mobile Robotics Program)
School of Electrical and Electronic Engineering
College of Engineering
Nanyang Technological University
Singapore
eswwijesoma@ntu.edu.sg

The Estimation Theoretic Sensor Bias Correction Problem in Map Aided Localization

Abstract

Simultaneous Localization and Map Building (SLAM) and Map Aided Localization (MAL) are very effective techniques employed extensively in robot navigation tasks. However, biases and drifts in both exteroceptive and proprioceptive sensors adversely impair correct localization (in MAL) and also impair map building (in SLAM). More specifically, accumulated errors as a result of biases in the sensors cause the algorithms to diverge and produce inconsistent and inaccurate results. Although offline calibration of these sensors can reduce the effects to some extent, the process results in longer setup and processing times. Moreover, during operation, the sensors' calibration may often be subject to changes or drifts requiring regular resetting and initialization. A convenient, appropriate and effective approach to overcome problems associated with biases in sensors has been to explicitly model and estimate the bias parameters concurrently with the vehicle state online using an augmented state space approach. This paper investigates the properties of the concurrent bias estimation in MAL using an augmented, estimation theoretic state space approach for the localization of a large class of mobile robots, consisting of autonomous ground vehicles. This involves a rigorous theoretical study of the issues of observability and convergence, their interrelations and effects on the algorithm's performance. This paper shows analytically that if sensor biases are estimated jointly with the vehicle pose in a MAL framework: 1) The uncertainties of the estimated errors in the bias parameters of both proprioceptive and exteroceptive sensors diminish in each update. 2) A derived lower bound is reached in each of these estimates. 3) The rate of convergence to this lower bound is also derived. 4) Although often neglected in the literature, observability is a major issue. From the analysis it is derived that in order to guarantee observability in MAL with bias estimation, it is necessary to observe simultaneously at least two distinct landmarks, which are not on a straight line with the vehicle position. Extensive simulations are provided to illustrate the theoretical results established for the general case of nonlinear dynamics and slowly varying sensor biases. The results are further exemplified and verified experimentally using a sophisticated MAL algorithm, utilizing a low cost inertial navigation sensor suite.

KEY WORDS—robot localization, map aiding, mapping

1. Introduction

The problem of positioning or localization is still considered to be one of the key challenges in achieving a truly autonomous navigation capability for mobile robots. Localization information is of paramount importance for any autonomous agent to plan missions, tasks or paths and execute any form of vehicle control (Durrant-Whyte 2001). In map aided localization (MAL), an a priori stored terrain map of some form is utilized in the localization algorithm. The platform with its onboard sensors, senses its surroundings, extracts salient features and compares them with the features in the stored map to find its current position. Application areas of MAL include reconnaissance and surveillance missions, guidance of weapons, mining, and cargo handling among many others. TERCOM (Hicks 1993), used in Cruise missile navigation, and TERPROM (Hosteler and Andreas 1983), used in low altitude aircraft navigation and collision avoidance, are two of the fully operational MAL systems currently available. These systems use an a priori digital terrain elevation map and data sensed by radar altimeters to provide corrections to an inertial navigation system (Hosteler and Andreas 1983). Although GPS-based location systems are very effective in open space, sea and air, they are affected by radio signal blockages and multi-path reflections off the ground and/or surrounding structures (buildings, canyon walls, etc.), partial satellite occlusion and active RF jamming. In such situations MAL can

The International Journal of Robotics Research
Vol. 25, No. 7, July 2006, pp. 645-667
DOI: 10.1177/0278364906066755

complement or substitute GPS-based location systems. The rich corpus of MAL literature contains several estimation algorithms including extended Kalman filters (EKF; Leonard and Durrant-Whyte 1991), particle filters (Fox et al. 1999), and transformation based filtering methods, which use only bearing information (Betke and Gurvits 1997; Briechle and Hanebeck 2004).

In this paper a rigorous theoretical investigation is carried out to understand the effects and implications of exteroceptive and proprioceptive sensor biases on map aided mobile robot localization in an estimation theoretic localization framework. In MAL, the propagation of sensor uncertainties due to systematic and nonsystematic errors may result in inconsistent and inaccurate localization results. Persistent and slowly varying biases due to modeling errors, sensor biases and imperfect calibrations may compromise performance. Use of linearized approximations of the nonlinear motion and sensor models and Gaussian assumptions in the measurement and process models also impair accurate and robust localization. Thus, biases in the sensors and modeling offsets and their cumulative effects can cause significant localization errors, especially over long operating hours and in large-scale outdoor MAL implementations.

There are several bias estimation methods proposed in the literature such as those of Krishnan and Grobert (1970), Fang and Wan (1996), Friedland (1969), and Ignagni (2000). Krishnan and Grobert (1970) and Fang and Wan (1996) used off-line inertial sensor calibration and error modeling approaches to offset the bias errors in the sensors. Friedland (1969) and Igangni (2000) presented effective techniques for separate bias estimation that are most suitable when the number of bias terms in the estimation process is high compared with the bias-free state vector. Huster and Rock (2003) described a relative position sensing strategy based on the nonlinear Unscented Kalman Filter that fuses bearing information from monocular vision, with inertial rate-sensor measurements to estimate relative velocity position and orientation. Although they explicitly accounted for the biases and random noises in the gyro (rate sensor) and accelerometers, a rigorous analysis of the properties and behavior of the estimator was difficult due to the nonlinear unscented transform utilized.

Martinelli et al. (2003) presented the theory and experimental results (using a differential drive robot) of simultaneous estimation of the robot configuration and the odometer error (both systematic and nonsystematic) during mobile robot navigation. Martinelli et al. (2003) described the notion of observability for a specific error model but did not investigate the algorithm properties rigorously. Roy and Thrun (1999) formulated the on-line self calibration problem of mobile robots as a maximum likelihood estimation problem and presented experimental results in an indoor setting. The sensor and measurement updates were calculated based on an occupancy grid based method. However, an occupancy grid based approach requires that different measurements obtained at the same instance be conditionally independent, which is not strictly true in MAL. Furthermore, it is not straightforward to evaluate the observability, convergence and other algorithmic properties of probabilistic occupancy grid based estimators. For mobile robots, Stroinger and Stone (2005) described a method to simultaneously learn the action and sensor models including their biases using linear regression techniques. However, the application of learning sensor and action models in MAL is not detailed.

The indirect approach to state estimation (Roumeliotis, Sukhatme, and Bekey 1999; Kim and Sukkarieh, 2004) is also a popular way of dealing with inertial navigation biases and drifts. The main advantage of the indirect formulation is that it gives a lesser number of predictions and linearized models. However, due to the inherent low dimensionality of the MAL problem, there is no definite computational or other advantage in the indirect form as compared with the direct form.

In this work an augmented state vector approach is used for sensor bias estimation and compensation because of its simplicity and low complexity when applied to the low dimensional MAL problem. The paper is organized as follows. In Section 2, MAL and the estimation theoretic bias correction problem in MAL are presented and discussed. In Section 3, the properties of the concurrent bias estimation and MAL algorithm are rigorously investigated and analyzed. In Section 4 extensive simulation results and experimental results are presented and discussed to validate the theoretical results established. Section 5 concludes the paper with a summary of the theoretical results and its implications on MAL.

2. Proprioceptive and Exteroceptive Sensor Bias Estimation

Section 2.1 gives an overview of the now standard EKF formulation used to estimate a vehicle's pose in MAL. For those familiar with this analysis, Section 2.1 can be skipped.

2.1. The Standard EKF/MAL

The basic EKF MAL framework represents the vehicle pose vector in absolute coordinates with reference to a global coordinate frame. That is, the state vector denoted by $\mathbf{X}(k)$ in this case consists only of the vehicle pose, $\mathbf{x}_v(k)$ at time k.

$$\mathbf{X}(k) = \mathbf{x}_v(k). \tag{1}$$

If the vehicle is assumed to be constrained to move on a two dimensional (2D) plane then the pose vector can be represented by $\mathbf{x}_v(k) = \begin{bmatrix} x(k) & y(k) & \theta(k) \end{bmatrix}^T$, where $x(k)$, $y(k)$ and $\theta(k)$ denote the Cartesian coordinates and heading of the vehicle with respect to the global reference coordinate frame as shown in Figure 1. The mid point of the rear axle of the vehicle represents the vehicle position. In general, the kinematic

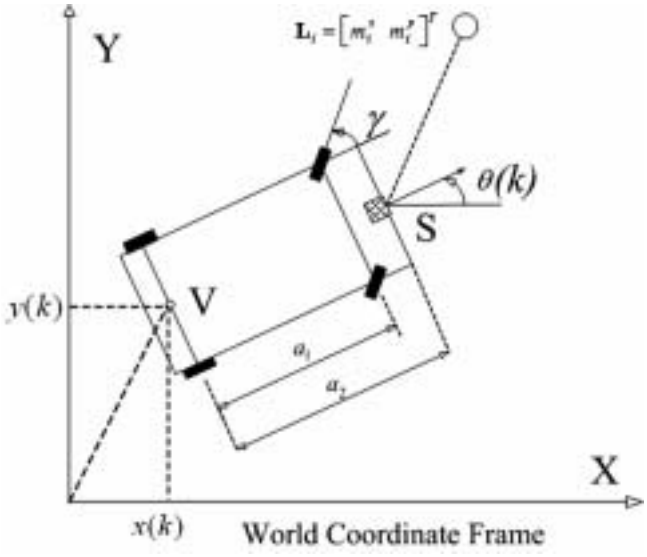

Fig. 1. The vehicle modeling and the coordinate frames.

motion model of the vehicle shown in Figure 1 is nonlinear and can be represented in closed form as

$$\begin{aligned}\mathbf{x}_v(k) &= \begin{bmatrix} x(k-1) + \Delta t\, u_a(k-1)\cos(\theta(k-1)) \\ y(k-1) + \Delta t\, u_a(k-1)\sin(\theta(k-1)) \\ \theta(k-1) + \Delta t\, u_a(k-1)\tan(\gamma_a(k-1))/a_1 \end{bmatrix} \\ &\quad + \mathbf{v}(k-1) \\ &= \mathbf{f}(\mathbf{x}_v(k-1), u_a(k-1), \gamma_a(k-1)) + \mathbf{v}(k-1),\end{aligned} \tag{2}$$

$$u_a(k-1) = u(k-1) + u_n(k-1), \tag{3}$$

$$\gamma_a(k-1) = \gamma(k-1) + \gamma_n(k-1). \tag{4}$$

Here $u(k-1)$ and $\gamma(k-1)$ denote the speed and the steering angle inputs at time $k-1$ respectively as measured by the proprioceptive sensors (e.g., odometers, gyroscopes etc.) and the lumped proprioceptive sensor input is expressed as $\mathbf{u}(k-1) = \begin{bmatrix} u(k-1) & \gamma(k-1) \end{bmatrix}^T$. $u_n(k) \sim N(0, \sigma_{u_n}^2)$ and $\gamma_n(k) \sim N(0, \sigma_{\gamma_n}^2)$, denote the random noises of u and γ which are assumed Gaussian with zero mean. The subscript "a" is used to denote the actual proprioceptive sensor inputs and a_1 is the vehicle wheel-base and Δt is the sampling time. $\mathbf{v}(k) \sim N(\mathbf{0}, \mathbf{Q}_v(k))$ is a temporally uncorrelated noise sequence with covariance matrix $\mathbf{Q}_v(k)$ representing the modeling uncertainties.

For simplicity, the landmarks in the environment are represented as point features. Thus the stored map is a vector $\mathbf{m}$ of n landmark points, $\mathbf{L}_i = \begin{bmatrix} m_i^x & m_i^y \end{bmatrix}^T$, $i = 1 \ldots n$, where (m_i^x, m_i^y) is the (x, y) coordinate pair of the ith landmark. Now if an exteroceptive sensor such as a laser range measurement system (e.g., SICK LMS 290) is used to observe the range and bearing of the ith landmark, we obtain the following observation model:

$$\begin{aligned}&\mathbf{z}(k) = \\ &\begin{bmatrix} \sqrt{(m_i^x - x_s(k))^2 + (m_i^y - y_s(k))^2} \\ \tan^{-1}\left((m_i^y - y_s(k))/(m_i^x - x_s(k))\right) + \pi/2 - \theta(k) \end{bmatrix} \\ &\quad + \mathbf{w}(k) = \mathbf{h}(\mathbf{x}_\mathbf{v}(k), \mathbf{L}_i) + \mathbf{w}(k)\end{aligned} \tag{5}$$

where $\mathbf{w}(k)$ is the vector of observation noise in range and bearing and is assumed Gaussian with zero mean and covariance $\mathbf{R}(k)$. $(x_s(k), y_s(k))$ is the absolute position of the exteroceptive sensor mounted on the vehicle at position S as shown in Figure 1 and is given by:

$$\begin{bmatrix} x_s(k) \\ y_s(k) \end{bmatrix} = \begin{bmatrix} x(k) + a_2\cos(\theta(k)) \\ y(k) + a_2\sin(\theta(k)) \end{bmatrix} \tag{6}$$

where a_2 is the offset of the exteroceptive sensor mounting from the vehicle reference position as shown in Figure 1. Now if the state covariance matrix of $\mathbf{X}(k-1)$ is $\mathbf{P}(k-1|k-1)$ at time $k-1$ then the EKF predictor equations are as follows:

$$\mathbf{X}(k|k-1) = \mathbf{x}_v(k|k-1) = \mathbf{f}(\mathbf{x}_v(k-1), \mathbf{u}(k-1)), \tag{7}$$

$$\mathbf{P}(k|k-1) = \mathbf{F}\mathbf{P}(k-1|k-1)\mathbf{F}^T + \mathbf{Q}(k-1), \tag{8}$$

$$\hat{\mathbf{z}}(k) = \mathbf{h}(\mathbf{x}_v(k|k-1), \mathbf{L}_i). \tag{9}$$

Here $\mathbf{F}$ is the Jacobian $(\partial\mathbf{f}/\partial\mathbf{X})$ of the process model evaluated at time $k-1$ and

$$\mathbf{Q}(k) = \left(\partial\mathbf{f}/\partial(u,\gamma)\right) diag(\sigma_{u_n}^2, \sigma_{\gamma_n}^2) \left(\partial\mathbf{f}/\partial(u,\gamma)\right)^T + \mathbf{Q}_v(k). \tag{10}$$

When the true observation $\mathbf{z}(k)$ is available at time k and after correct observations to map feature associations are resolved using an appropriate data association algorithm, the EKF update equations are applied as follows:

$$\mathbf{e}(k) = \mathbf{z}(k) - \hat{\mathbf{z}}(k), \tag{11}$$

$$\mathbf{X}(k|k) = \mathbf{X}(k|k-1) + \mathbf{K}(k)\mathbf{e}(k), \tag{12}$$

$$\mathbf{P}(k|k) = \mathbf{P}(k|k-1) - \mathbf{K}(k)\mathbf{S}(k)\mathbf{K}^T(k), \tag{13}$$

where $\mathbf{e}(k)$, $\mathbf{S}(k)$, $\mathbf{H}$ and $\mathbf{K}(k) = \mathbf{P}(k|k-1)\mathbf{H}^\mathbf{T}\mathbf{S}^{-\mathbf{1}}(k)$ denote respectively the observation innovation, its covariance matrix, the Jacobian $(\partial\mathbf{h}/\partial\mathbf{X})$ and the Kalman gain with the usual notation.

2.2. Concurrent Bias Estimation with MAL

Although offline calibration and modeling of biases in sensors can reduce or mitigate localization errors to some extent, these processes result in longer setup and processing times. Moreover, during operation, the sensors' calibration may often be subject to changes or drifts requiring regular resetting and initialization. A convenient, appropriate and an effective way to overcome problems associated with biases in sensors is to explicitly model and estimate the bias parameters online, jointly with the vehicle state. Work described here aims to investigate the properties of this augmented estimation theoretic state space approach to joint estimation of biases and vehicle state in map aided localization for a large class of mobile robots, consisting of autonomous ground vehicles. This includes a rigorous theoretical analysis on the issues of observability and convergence, their interrelations and effects on the algorithm's performance.

To better appreciate the joint estimation of biases in the sensors and vehicle state in MAL, consider the problem of one degree-of-freedom (1D) MAL. Here, a vehicle traversing a straight line path (along the x-axis) attempts to localize itself on a straight line based on the correct association of landmarks observed on the line with those stored in an a priori map $\mathbf{m}$. If the vehicle's proprioceptive and exteroceptive sensors' biases are $u_b(k)$ and $s_b(k)$ at time k respectively, then the process (incorporating the biases) and the measurement models of the 1D problem, when observing a single known (or stored) landmark, are given by

$$\mathbf{X}(k) = \begin{bmatrix} 1 & 1 & 0 \\ 0 & 1 & 0 \\ 0 & 0 & 1 \end{bmatrix} \mathbf{X}(k-1) + \begin{bmatrix} u(k-1) \\ 0 \\ 0 \end{bmatrix} + \begin{bmatrix} v(k-1) \\ 0 \\ 0 \end{bmatrix}, \tag{14}$$

$$z(k) = \begin{bmatrix} -1 & 0 & 1 \end{bmatrix} \mathbf{X}(k) + L + w(k). \tag{15}$$

Here, $\mathbf{X}(k) = \begin{bmatrix} x_v(k) & u_b(k) & s_b(k) \end{bmatrix}^T$ is the joint or augmented state vector including vehicle state and biases in the sensors. $v(k) \sim N(0, q^2)$, and $w(k) \sim N(0, r^2)$ are the exteroceptive and proprioceptive sensor noises assumed Gaussian with zero means and variances q^2 and r^2 respectively. L is the coordinates of the observed known or stored landmark.

Now, by extending the derivations given in Section 2.1, we formulate the concurrent bias estimation of exteroceptive and proprioceptive sensors with vehicle state for the more realistic 2D MAL problem. Again for simplicity we consider only a single exteroceptive sensor for making observations of landmarks, although the derivation that follows can be extended to any arbitrary number. Let the lumped proprioceptive sensor biases, namely the biases in the input vehicle speed and input steering angle, be $u_b(k)$ and $\gamma_b(k)$. Suppose that the exteroceptive sensor's biases in the range and bearing are $r_b(k)$ and $\alpha_b(k)$ respectively. By incorporating all of the biases of both proprioceptive and exteroceptive sensors, we form the vector of biases $\mathbf{x}_b(k)$ as follows:

$$\mathbf{x}_b(k) = \begin{bmatrix} u_b(k) & \gamma_b(k) & r_b(k) & \alpha_b(k) \end{bmatrix}^T. \tag{16}$$

As was illustrated for the 1D case for online concurrent bias and vehicle state estimation and filtering in MAL, a new composite state vector $\mathbf{X}$ is formed by concatenating the vehicle state vector and the vector of biases as follows:

$$\mathbf{X}(k) = \begin{bmatrix} \mathbf{x}_v^T(k) & \mathbf{x}_b^T(k) \end{bmatrix}^T. \tag{17}$$

The new vehicle model takes the form of (2) with changes to $u_a(k-1)$ and $\gamma_a(k-1)$ as follows:

$$u_a(k-1) = u(k-1) + u_n(k-1) + u_b(k-1), \tag{18}$$

$$\gamma_a(k-1) = \gamma(k-1) + \gamma_n(k-1) + \gamma_b(k-1). \tag{19}$$

We assume that the biases of the proprioceptive sensors exhibit a random walk behavior and that those of the exteroceptive sensors are constant. Thus we have

$$u_b(k) = u_b(k-1) + u_{b_n}(k-1), \tag{20}$$

$$\gamma_b(k) = \gamma_b(k-1) + \gamma_{b_n}(k-1), \tag{21}$$

$$r_b(k) = r_b(k-1), \tag{22}$$

$$\alpha_b(k) = \alpha_b(k-1), \tag{23}$$

where $u_{b_n} \sim N(0, \sigma_{ub}^2)$ and $\gamma_{b_n} \sim N(0, \sigma_{\gamma b}^2)$. Now the time evolution of the concatenated bias state vector which is assumed to exhibit a random walk behavior can be expressed as

$$\mathbf{x}_b(k) = \mathbf{x}_b(k-1) + \mathbf{v}_b(k-1) \tag{24}$$

where $\mathbf{v}_b(k) \sim N(\mathbf{0}, diag(\sigma_{u_{nb}}^2, \sigma_{\gamma_{nb}}^2, 0, 0))$ and $\sigma_{u_{nb}}^2$ and $\sigma_{\gamma_{nb}}^2$ are assumed to be the known variances of $u_{b_n}(k)$ and $\gamma_{b_n}(k)$ respectively. If the biases are known to behave differently, then it is straightforward to incorporate their different time varying characteristics in the formulation through appropriate modeling.

The observation model when modified to incorporate the biases of the exteroceptive sensors becomes:

$$\begin{aligned} \mathbf{z}(k) &= \mathbf{h}(\mathbf{x}_v(k), x_i(k), y_i(k)) + [r_b(k)\ \alpha_b(k)]^T + \mathbf{w}(k) \\ &= \mathbf{h}(\mathbf{x}_v(k), x_i(k), y_i(k), r_b(k), \alpha_b(k)) + \mathbf{w}(k). \end{aligned} \tag{25}$$

Now the concurrent estimation of the bias parameters with the vehicle state in MAL proceeds according to (7) to (13),

with the augmented vehicle and bias model (17) to (24) and the observation model (25) replacing (2) and (5) respectively. It may be noted that the system of eqs (18) to (25) describing concurrent bias estimation with the vehicle state in MAL is nonlinear. To develop insight and facilitate theoretical analysis (Section 3) the system of eqs (16) to (25) is first linearized as follows:

$$\mathbf{X}(k) = \begin{bmatrix} \partial \mathbf{f}_v / \partial \mathbf{x}_v & \partial \mathbf{f} / \partial \mathbf{x}_b \\ \mathbf{0}_{4\times 3} & \mathbf{I}_{4\times 4} \end{bmatrix} \begin{bmatrix} \mathbf{x}_v(k-1) \\ \mathbf{x}_b(k-1) \end{bmatrix} + \begin{bmatrix} \partial \mathbf{f}_v / \partial \mathbf{u} \\ \mathbf{0}_{4\times 2} \end{bmatrix} \mathbf{u}_a(k-1) + \begin{bmatrix} \mathbf{v}^T(k-1) & \mathbf{v}_b^T(k-1) \end{bmatrix}^T + \mathbf{d}_f(k), \quad (26)$$

$$\mathbf{z}(k) = \begin{bmatrix} \partial \mathbf{h} / \partial \mathbf{x}_v & \partial \mathbf{h} / \partial \mathbf{x}_b \end{bmatrix} \begin{bmatrix} \mathbf{x}_v^T(k) & \mathbf{x}_b^T(k) \end{bmatrix}^T + \mathbf{w}(k) + \mathbf{d}_h(k), \quad (27)$$

where $\mathbf{u}_a(k-1) = \begin{bmatrix} u_a(k-1) & \gamma_a(k-1) \end{bmatrix}^T$. $\mathbf{0}_{n\times m}$ is the null matrix of dimension $n\times m$ and $\mathbf{I}_{n\times n}$ is the identity matrix of dimension $n\times n$. Here, n and m are non-zero integers. The quantities $\mathbf{d}_f(k)$ and $\mathbf{d}_h(k)$ can be determined from the following equations:

$$\mathbf{d}_f(k) = \mathbf{f}(\hat{\mathbf{x}}_v(k-1), \hat{u}_b(k-1), \hat{\gamma}_b(k-1), \mathbf{u}(k-1)) - \begin{bmatrix} \partial \mathbf{f}_v / \partial \mathbf{x}_v & \partial \mathbf{f}_v / \partial \mathbf{x}_b \\ \mathbf{0}_{4\times 3} & \mathbf{I}_{4\times 4} \end{bmatrix} \begin{bmatrix} \hat{\mathbf{x}}_v(k-1) \\ \hat{\mathbf{x}}_b(k-1) \end{bmatrix} - \begin{bmatrix} \left(\partial \mathbf{f}_v / \partial \mathbf{u}\right)^T & \mathbf{0}_{2\times 4} \end{bmatrix}^T \mathbf{u}(k-1), \quad (28)$$

$$\mathbf{d}_h(k) = \mathbf{h}(\hat{\mathbf{x}}_v(k), \mathbf{L}_i, \hat{r}_b(k), \hat{\alpha}_b(k)) - \begin{bmatrix} \partial \mathbf{h} / \partial \mathbf{x}_v & \partial \mathbf{h} / \partial \mathbf{x}_b \end{bmatrix} \begin{bmatrix} \hat{\mathbf{x}}_v^T(k) & \hat{\mathbf{x}}_b^T(k) \end{bmatrix}^T, \quad (29)$$

where the quantities $\hat{\mathbf{x}}_v(k-1)$, $\hat{\mathbf{x}}_\mathbf{b}(k-1)$, $\hat{u}_b(k-1)$, $\hat{\gamma}_b(k-1)$, $\hat{\mathbf{x}}_\mathbf{v}(k)$, $\hat{\mathbf{x}}_b(k)$, $\hat{r}_b(k)$ and $\hat{\alpha}_b(k)$ denote the estimates of the states $\mathbf{x_v}$, $\mathbf{x_b}$, u_b and γ_b at time $k-1$ and the predictions of the states $\mathbf{x_v}$, $\mathbf{x_b}$, r_b and α_b at time $k$respectively given the states at time $k-1$ and $\mathbf{f}(.) = [(\mathbf{f}_v(.))^T \mathbf{x}_b^T(k-1)]^T$.

It may be noted that the linearized eqs (26) to (29) have the same general structure as the simple linear bias estimation algorithm for the linear MAL case.

3. Analysis of the Bias Estimation Problem in MAL

Previous work on MAL (Leonard and Durrant-Whyte 1991; Fox et al. 1999; Durrant-Whyte 2001) has mostly emphasized the formulation and application of MAL in mobile robotics. However, the observability, convergence and bounds of uncertainty of the estimated bias parameters are major concerns of MAL in practice and require greater attention.

3.1. Diminishing Uncertainty of Bias Estimates

Whether it be the ideal 1D linear case ((14) and (15)) or the more realistic 2D nonlinear case (linearized models given by (26) to (29)), for the case of constant biases (where $\sigma_{ub}^2 = \sigma_{\gamma b}^2 = 0$), we can summarize the problem of the joint estimation of the biases with the vehicle state in MAL in the following manner. If $\mathbf{u}_b(k)$ and $\mathbf{s}_b(k)$ are used to denote the proprioceptive and exteroceptive sensors' bias vectors respectively then the bias vector of (16) $\mathbf{x}_b(k)$ can be concisely expressed as follows:

$$\mathbf{x}_b(k) = \begin{bmatrix} \mathbf{u}_b^T(k) & \mathbf{s}_b^T(k) \end{bmatrix}^T = \mathbf{x}_b(k-1). \quad (30)$$

The evolution of the composite state vector $\mathbf{X}(k)$ given by (17), comprising the bias vector $\mathbf{x}_b(k)$ and the vehicle state $\mathbf{X}_v(k)$ can be expressed as

$$\mathbf{X}(k) = \mathbf{F}\mathbf{X}(k-1) + \mathbf{B}_v\mathbf{u}(k-1) + [\mathbf{v}^T(k)\ \mathbf{0}]^T \quad (31)$$

where $\mathbf{B}_v$ is the transition matrix of the proprioceptive sensor measurements, $\mathbf{v}(k)$ and $\mathbf{u}(k)$ are defined in Section 2.1. The matrix $\mathbf{F}$ is

$$\mathbf{F} = \begin{bmatrix} \mathbf{F}_v & \mathbf{B}_v & \mathbf{0}_{vs} \\ \mathbf{0}_{vu}^T & \mathbf{I}_{uu} & \mathbf{0}_{us} \\ \mathbf{0}_{vs}^T & \mathbf{0}_{us}^T & \mathbf{I}_{ss} \end{bmatrix} \quad (32)$$

where $\mathbf{I}_{ss}$ and $\mathbf{I}_{uu}$ are identity matrices with dimensions $\dim(\mathbf{s}_b)\times\dim(\mathbf{s}_b)$ and $\dim(\mathbf{u}_b)\times\dim(\mathbf{u}_b)$ respectively. $\mathbf{0}_{vs}$, $\mathbf{0}_{vu}$ and $\mathbf{0}_{us}$ are null matrices having appropriate dimensions. The observation model corresponding to (15) and (27) can be expressed as:

$$\mathbf{z}(k) = \mathbf{H}(k)\mathbf{X}(k) + \mathbf{L} + \mathbf{w}(k) \quad (33)$$

where, $\mathbf{H}(k) = \begin{bmatrix} -\mathbf{H}_v(k) & \mathbf{0}_{uu} & \mathbf{I}_{ss} \end{bmatrix}$, with $\mathbf{L}$ denoting a constant vector corresponding to the observed landmark in the stored map and $\mathbf{w}(k) \sim N(\mathbf{0}, \mathbf{R}(k))$ denotes the observation noise. $\mathbf{0}_{uu}$ is a null matrix of dimension $\dim(\mathbf{u}_b)\times\dim(\mathbf{u}_b)$. Then the prediction and update equations take the form of (7) to (13) with the process and observation models (31) and (33) replacing those given in the general formulation outlined in the previous section. Now, if $\mathbf{P}(k|k)$ represents the covariance matrix of the composite state vector $\mathbf{X}(k)$, it can be partitioned

as follows:

$$\mathbf{P}(k|k) = \begin{bmatrix} \mathbf{P}_{vv}(k|k) & \mathbf{P}_{vu}(k|k) & \mathbf{P}_{vs}(k|k) \\ \mathbf{P}_{vu}^T(k|k) & \mathbf{P}_{uu}(k|k) & \mathbf{P}_{us}(k|k) \\ \mathbf{P}_{vs}^T(k|k) & \mathbf{P}_{us}^T(k|k) & \mathbf{P}_{ss}(k|k) \end{bmatrix} \quad (34)$$

where the subscripts v, u, and s denote the vehicle state, proprioceptive sensor and exteroceptive sensor bias vectors respectively. For example, $\mathbf{P}_{vv}(k|k)$ denotes the vehicle state's covariance and $\mathbf{P}_{vs}(k|k)$ denotes the cross covariance of vehicle state and the exteroceptive sensor bias state. Now from (8), the prediction of the composite state vector covariance matrix $\mathbf{P}(k|k-1)$ can be determined. Let $\mathbf{P}(k|k-1)$be partitioned as follows:

$$\mathbf{P}(k|k-1) = \begin{bmatrix} \mathbf{P}_1 & \mathbf{P}_4 & \mathbf{P}_5 \\ \mathbf{P}_4^T & \mathbf{P}_2 & \mathbf{P}_6 \\ \mathbf{P}_5^T & \mathbf{P}_6^T & \mathbf{P}_3 \end{bmatrix}.$$

Then it follows that

$$\begin{aligned} \mathbf{P}_1 = {} & \mathbf{F}_v\mathbf{P}_{vv}(k-1|k-1)\mathbf{F}_v^T + \mathbf{F}_v\mathbf{P}_{vu}(k-1|k-1)\mathbf{B}_v^T \\ & + \mathbf{B}_v\mathbf{P}_{uu}(k-1|k-1) + \mathbf{B}_v\mathbf{P}_{vu}(k-1|k-1)\mathbf{B}_v^T \\ & + \mathbf{F}_v\mathbf{P}_{vu}(k-1|k-1) + \mathbf{Q}_v(k), \end{aligned} \quad (35)$$

$$\mathbf{P}_2 = \mathbf{P}_{uu}(k-1|k-1), \quad (36)$$

$$\mathbf{P}_3 = \mathbf{P}_{ss}(k-1|k-1), \quad (37)$$

$$\mathbf{P}_4 = \mathbf{F}_v\mathbf{P}_{vu}(k-1|k-1) + \mathbf{B}_v\mathbf{P}_{uu}(k-1|k-1), \quad (38)$$

$$\mathbf{P}_5 = \mathbf{F}_v\mathbf{P}_{vs}(k-1|k-1) + \mathbf{B}_v\mathbf{P}_{us}(k-1|k-1), \quad (39)$$

$$\mathbf{P}_6 = \mathbf{P}_{us}(k-1|k-1). \quad (40)$$

As $\mathbf{P}(0|0)$, $\mathbf{Q}(k)$ and $\mathbf{R}(k)$ are positive semi definite (PSD) matrices, by the properties (Horn and Johnson 1985) of PSD matrices (see Appendix), $\mathbf{S}(k)$ and $\mathbf{K}(k)\mathbf{S}(k)\mathbf{K}^T(k)$ are also PSD matrices. Hence from (13),

$$\det(\mathbf{P}(k|k)) = \det\left(\mathbf{P}(k|k-1) - \mathbf{K}(k)\mathbf{S}(k)\mathbf{K}^T(k)\right), \quad (41)$$

$$\det(\mathbf{P}(k|k)) \leqslant \det(\mathbf{P}(k|k-1)). \quad (42)$$

Since any principal sub matrix of a PSD matrix is also PSD,

$$\det(\mathbf{P}_{uu}(k|k)) \leqslant \det(\mathbf{P}_{uu}(k|k-1)), \quad (43)$$

$$\det(\mathbf{P}_{ss}(k|k)) \leqslant \det(\mathbf{P}_{ss}(k|k-1)). \quad (44)$$

However, from (36) and (37), $\mathbf{P}_{uu}(k|k-1) = \mathbf{P}_{uu}(k-1|k-1)$ and $\mathbf{P}_{ss}(k|k-1) = \mathbf{P}_{ss}(k-1|k-1)$. Therefore from (43) and (44),

$$\det(\mathbf{P}_{uu}(k|k)) \leqslant \det(\mathbf{P}_{uu}(k-1|k-1)), \quad (45)$$

$$\det(\mathbf{P}_{ss}(k|k)) \leqslant \det(\mathbf{P}_{ss}(k-1|k-1)). \quad (46)$$

Since the determinant of a matrix is proportional to its volume, the determinants of the covariance matrices indicate the volume or size of their uncertainty ellipses and therefore it can be concluded that the errors in the estimates of the bias parameters involving both proprioceptive and exteroceptive sensors diminish in each successive update ((45) and (46) of the MAL algorithm). This is an important result and its implications involving nonlinear models are further investigated in Section 4.

3.2. Lower Bounds of the Uncertainty

In this section we investigate rigorously whether the decrease in the bias estimation errors over successive observations as shown in the Section 3.1 will eventually become zero (biases completely determined with no uncertainty) or approach a non-zero but finite lower limit. It may be noted that the lowest covariance estimate is obtained when the proprioceptive sensor noise and the modeling uncertainty (process noise) are at their minima (i.e., when $\mathbf{Q}$ is lowest) and the observation noise is small. Such a scenario occurs when the vehicle is stationary ($\mathbf{Q} = \mathbf{0}$) whilst observing a landmark in the stored map. However, under these circumstances it is not possible to obtain an estimate of the proprioceptive sensor bias terms as they are not observable when the vehicle is not in motion. Hence we calculate the lower bounds for the covariance of the exteroceptive sensor bias vector $\mathbf{s}_b$ when the vehicle is stationary. In this situation, the composite state vector reduces to:

$$\mathbf{X}(k) = \begin{bmatrix} \mathbf{x}_v^T(k) & \mathbf{s}_b^T(k) \end{bmatrix}^T. \quad (47)$$

The observation model takes the form of (33) with $\mathbf{H}(k) = \begin{bmatrix} -\mathbf{H}_v(k) & \mathbf{I}_{ss} \end{bmatrix}$. Since the vehicle is stationary, the predicted covariance matrix $\mathbf{P}(k|k-1)$ for all k is

$$\mathbf{P}(k|k-1) = \mathbf{P}(k-1|k-1). \quad (48)$$

Suppose the initial value of the covariance matrix is $\mathbf{P}(0|0) = diag(\mathbf{P}_v, \mathbf{P}_b)$, where $\mathbf{P}_v$ and $\mathbf{P}_b$ denote the initial covariance matrices of the vehicle and the exteroceptive sensor biases respectively. Using the inverse covariance form of the Kalman filter (Brown and Hwang 1992; Bar-Shalom and Li 2001),

$$\mathbf{P}^{-1}(k|k) = \mathbf{P}^{-1}(k|k-1) + \mathbf{H}^T\mathbf{R}^{-1}\mathbf{H}. \quad (49)$$

Hence when making k observations,

$$\mathbf{P}^{-1}(k|k) = \begin{bmatrix} \mathbf{P}_v^{-1} + k\mathbf{H}_v^T\mathbf{R}^{-1}\mathbf{H}_v & -k\mathbf{H}_v^T\mathbf{R}^{-1} \\ -k\mathbf{R}^{-1}\mathbf{H}_v & \mathbf{P}_b^{-1} + k\mathbf{R}^{-1} \end{bmatrix} = \begin{bmatrix} \mathbf{A} & \mathbf{B} \\ \mathbf{C} & \mathbf{D} \end{bmatrix}. \quad (50)$$

Let $\mathbf{P}(k|k) = \begin{bmatrix} \mathbf{A} & \mathbf{B} \\ \mathbf{C} & \mathbf{D} \end{bmatrix}^{-1} = \begin{bmatrix} \mathbf{P}_{11} & \mathbf{P}_{12} \\ \mathbf{P}_{21} & \mathbf{P}_{22} \end{bmatrix}$ where $\mathbf{P}_{22}$ is the covariance matrix of the exteroceptive sensor biases. Thus using $\mathbf{P_{11}} = (\mathbf{A} - \mathbf{BD}^{-1}\mathbf{C})^{-1}$ and similar identities it can be shown that:

$$\mathbf{P}_{11} = (\mathbf{P}_v^{-1} + k\mathbf{H}_v^T\mathbf{R}^{-1}\mathbf{H}_v - k\mathbf{H}_v^T\mathbf{R}^{-1} (\mathbf{P}_b^{-1} + k\mathbf{R}^{-1})^{-1}k\mathbf{R}^{-1}\mathbf{H}_v)^{-1}, \quad (51)$$

$$\mathbf{P}_{12} = (\mathbf{P}_v^{-1} + k\mathbf{H}_v^T\mathbf{R}^{-1}\mathbf{H}_v)^{-1}(-k\mathbf{H}_v^T\mathbf{R}^{-1})((k\mathbf{R}^{-1}\mathbf{H}_v) (\mathbf{P}_v^{-1} + k\mathbf{H}_v^T\mathbf{R}^{-1}\mathbf{H}_v)^{-1}(k\mathbf{H}_v^T\mathbf{R}^{-1}) - (\mathbf{P}_b^{-1} + k\mathbf{R}^{-1}))^{-1}, \quad (52)$$

$$\mathbf{P}_{21} = \mathbf{P}_{12}^T, \quad (53)$$

$$\mathbf{P}_{22} = (\mathbf{P}_b^{-1} + k\mathbf{R}^{-1} - k^2\mathbf{R}^{-1}\mathbf{H}_v (\mathbf{P}_v^{-1} + k\mathbf{H}_v^T\mathbf{R}^{-1}\mathbf{H}_v)^{-1}\mathbf{H}_v^T\mathbf{R}^{-1})^{-1}. \quad (54)$$

Since the value of $\mathbf{P}_{22}$ is obtained by assuming zero vehicle and proprioceptive sensor uncertainties, its inverse represents the maximum information gain conceivable or realizable for the algorithm. In the limit when a large number of successive observations are made using on board sensors while the vehicle is stationary, the upper limit of this information gain will be reached (if a limit exists at all). Conversely, if this finite limit exists the covariance of the exteroceptive sensor bias term $\mathbf{P}_{22}$ will reach its lower bound. Therefore this limit, if it exists, is a lower bound $\mathbf{P}_{\mathbf{22}}^*$ for the covariance $\mathbf{P}_b(k|k)$ of the exteroceptive sensor bias term under the given circumstances, i.e.,

$$\mathbf{P}_{\mathbf{22}}^* = \lim_{k\to\infty}(\mathbf{P}_{22}). \quad (55)$$

The lower bound of the covariance (given by (55)) of the exteroceptive sensor biases can be obtained in closed form for the special cases given below.

Case 1: The initial uncertainty of exteroceptive sensor biases is infinite, i.e., the biases are completely unknown. From (51) to (55),

$$\mathbf{P}_b(k|k) = \lim_{\mathbf{P}_b\to\infty}(\mathbf{P}_{22}^*) = \mathbf{H}_v\mathbf{P}_v\mathbf{H}_v^T. \quad (56)$$

Therefore, when the bias terms are initially completely unknown the lower bound of the uncertainty of the exteroceptive sensor biases is $\mathbf{H}_v\mathbf{P}_v\mathbf{H}_v^T$. Hence, the lower bound of uncertainty of the exteroceptive sensor's biases is determined by the initial covariance of the vehicle pose or in other words the covariance of the vehicle ($\mathbf{P}_v$). On the other hand, if the vehicle's starting position is initially known with complete certainty then $\mathbf{P}_b(k|k)$ should reach zero or a value independent of the initial conditions depending on observability conditions.

Case 2: If the vehicle's initial position is completely unknown, such as in the Kidnapped Robot Problem, then $\mathbf{P}_v \to \infty$. i.e., $\mathbf{P}_v^{-1} = 0$. After careful rearrangement of terms and simplification of eqs (50) to (56), it can be shown that

$$\mathbf{P}_{22} = \mathbf{P}_b. \quad (57)$$

Hence, $\mathbf{P}_b(k|k) = \mathbf{P}_b$ for all k.This implies that the uncertainty of the exteroceptive sensor biases cannot be reduced by observing a known landmark from an unknown vehicle position while the vehicle is stationary.

These observations can be reiterated for a situation involving a single degree of freedom MAL problem. Consider the simplified process and observation models derived in (14) and (15) and the removal of the proprioceptive bias term in the state vector as follows:

$$\mathbf{X}(k) = \begin{bmatrix} x_v(k) & s_b(k) \end{bmatrix}^T, \quad (58)$$

$$z(k) = \begin{bmatrix} -1 & 1 \end{bmatrix}\begin{bmatrix} x_v(k) & s_b(k) \end{bmatrix}^T + L. \quad (59)$$

By comparing (59) with (33), it may be deduced that in this case $\mathbf{H} = \begin{bmatrix} -1 & 1 \end{bmatrix}$, and $\mathbf{H_v} = 1$. Now, using the scalar forms of uncertainties for the initial covariance matrix of $\mathbf{X}(k)$, given by $\mathbf{P}(0|0) = diag(P_v, P_b)$ and using the standard inverse covariance form of the Kalman filter given by (49),

$$\mathbf{P}(k|k) = \frac{1}{R + kP_b + kP_v}\begin{bmatrix} (R + kP_b)P_v & kP_vP_b \\ kP_vP_b & (R + kP_v)P_b \end{bmatrix}, \quad (60)$$

$$P_b(\infty) = \lim_{k\to\infty}\frac{(R + kP_v)P_b}{R + kP_b + kP_v} = \frac{P_vP_b}{P_b + P_v}, \quad (61)$$

where $P_b(\infty)$ is the steady state error covariance of the exteroceptive sensor bias term for the single degree of freedom MAL algorithm. The decrease in the bias variance $\delta P_b(\infty)$ is given by:

$$\delta P_b(\infty) = \lim_{k\to\infty}\left(P_b - \frac{(R + kP_v)P_b}{R + kP_b + kP_v}\right) = \frac{P_b^2}{P_b + P_v} > 0. \quad (62)$$

Equation (62) suggests that, in the limit, the exteroceptive sensor bias variance is strictly monotonically decreasing and is bounded by (61).

3.3. Observability Conditions

It is always important to know how the choice or design of observation model and constraints for a given process model influences the observability of the estimated states. In the following, we analyze the observability conditions of several scenarios in MAL to gain insight, assess and improve the performance of the estimator. First we analyze the observability of the 1D MAL formulation where n landmarks are observed with biased proprioceptive and exteroceptive sensors. Upon writing process and observation equations (14) and (15) in terms of their linearized error states we obtain:

$$\tilde{\mathbf{X}}(k) = \mathbf{F}\tilde{\mathbf{X}}(k-1) + \mathbf{B}\left[\, v(k-1) \quad \mathbf{0}_{1\times 2} \quad [w_1\ w_2 \ldots w_n] \,\right]^T, \tag{63}$$

$$\tilde{\mathbf{z}}(k) = \mathbf{H}\tilde{\mathbf{X}}(k) + \mathbf{H}_w\left[\, v(k-1) \quad \mathbf{0}_{1\times 2} \quad [w_1\ w_2\ \mathbf{...}\ w_n] \,\right]^T, \tag{64}$$

where $\left[\, v(k-1) \quad \mathbf{0}_{1\times 2} \quad [w_1\ w_2\ \mathbf{...}\ w_n] \,\right]$ is the input noise vector written in terms of the concatenated process and measurement noise terms,

$$\mathbf{H} = [-\mathbf{1}_{n\times 1}\ \mathbf{0}_{n\times 1}\ \mathbf{1}_{n\times 1}],$$

$$\mathbf{H}_w = \left[\, \mathbf{0}_{n\times 3} \quad \mathbf{I}_{n\times n} \,\right], \quad \mathbf{F} = \begin{bmatrix} 1 & 1 & 0 \\ 0 & 1 & 0 \\ 0 & 0 & 1 \end{bmatrix},$$

$$\mathbf{B} = \begin{bmatrix} 1 & \mathbf{0}_{1\times(n+2)} \\ \mathbf{0}_{(n+2)\times 1} & \mathbf{0}_{(n+2)\times(n+2)} \end{bmatrix}$$

and $\mathbf{(1)}_{n_1\times n_2}$ is a matrix of size $n_1 \times n_2$ with all elements equal to one.

Now it is possible to compute the observability and controllability Grammians, $\mathbf{G_O}$ and $\mathbf{G_C}$ respectively. For linear time invariant systems such as (63) and (64), $\mathbf{G_O}$ and $\mathbf{G_C}$ can be determined as follows:

$$\mathbf{G_O} = \left[(\mathbf{HF})^T\ (\mathbf{HF^2})^T \ldots\ldots (\mathbf{HF}^i)^T\right]^T, \tag{65}$$

$$\mathbf{G_C} = \left[\mathbf{B}\ \mathbf{FB}\ \mathbf{F}^2\mathbf{B} \ldots\ldots \mathbf{F}^{i-1}\mathbf{B}\right], \tag{66}$$

where i is the dimension of the state vector $\tilde{\mathbf{X}}(k)$. The system is controllable if $\mathbf{G_C}$ has a column rank of i and observable if $\mathbf{G_O}$ has a row rank of i.

Hence from (63) and (64) it is clear that the rank of $\mathbf{G_O}$ is two and thus it is rank deficient by one. Therefore, the sensor bias estimation problem in 1D MAL is partially observable. The second case arises when the bias in the vehicle's speed proprioceptive measurement has a random walk behavior as modeled by (20). In this case, $\mathbf{X}(k)$, $\mathbf{F}$, $\mathbf{H}$ and $\mathbf{z}(k)$ take the same form as in the previous system ((63) and (64)) with changes in,

$$\tilde{\mathbf{X}}(k) = \mathbf{F}\tilde{\mathbf{X}}(k-1) + \mathbf{B}\left[v(k)\ v_b(k)\ \mathbf{0}_{1\times(n+1)}\right]^T \tag{67}$$

and

$$\mathbf{B} = \begin{bmatrix} 1 & 0 & \mathbf{0}_{1\times(n+1)} \\ 0 & 1 & \mathbf{0}_{1\times(n+1)} \\ \mathbf{0}_{(n+1)\times 1} & \mathbf{0}_{(n+1)\times 1} & \mathbf{0}_{(n+1)\times(n+1)} \end{bmatrix}.$$

In this case, the rank of $\mathbf{G_O}$ is two, i.e., rank deficient by one. However, the rank of $\mathbf{G_C}$ in this case is two, which is higher than the rank of $\mathbf{G_C}$ in the previous case with the constant bias term. The results also show that the angle between the controllable and observable subspaces in the previous case is $\pi/2$ and in this case is $\pi/4$. This implies that corrections to the state estimate driven by exteroceptive sensor measurement noise could reconstruct the vehicle state more accurately when the biases are variable as opposed to constant. If the MAL formulation is partially observable there is a possibility that the uncertainty in an estimation algorithm may increase in an unobservable direction. However, according to the analysis on diminishing uncertainties in Section 3.1, the direction of degeneracy is not possible along the biases as uncertainties of biases decrease in each update. Thus, the degeneracy can possibly occur in the direction of the robot position, resulting in inaccurate localization. This partial observability situation in 1D MAL can be rectified by incorporating absolute position information of the vehicle in the measurement vector. Thus the observation matrix, $\mathbf{H}$ of the fully observable, ID MAL formulation with sensor biases and observation of n known landmarks is:

$$\mathbf{H} = \begin{bmatrix} -\mathbf{1}_{n\times 1} & \mathbf{0}_{n\times 1} & \mathbf{1}_{n\times 1} \\ 1 & 0 & 0 \end{bmatrix}. \tag{68}$$

In general there are no specific rules governing the observability of nonlinear stochastic systems and therefore, it is difficult to have prior judgments on the viability of 2D MAL with concurrent sensor bias estimation, which is inherently nonlinear. However, a test similar to the observability analysis of linear systems may be carried out by linearizing the nonlinear process and observation models about a state (Southall, Buxton, and Marchant 1998; Reif et al. 1999). Here the rank test is carried out on an observation matrix constructed from the Jacobians of the process and observation models which are assumed piecewise constant. Although this rank analysis is not always sufficient to ensure observability, it provides the necessary conditions (Reif et al. 1999).

The observability analysis of the planar (2D) nonlinear MAL algorithm is carried out by symbolic manipulation of models (16) to (25) with a single known landmark observation. The analysis shows that the observability matrix is rank deficient by 2 (the dimension of the state vector is 7, and the rank of $\mathbf{G_O}$ is 5). However, it can be shown that the matrix $\mathbf{G_O}$ becomes full rank when observing more than one known landmark at the same time. Hence, for observability in 2D MAL, with bias estimation, it is a pre-requisite that at least two landmarks are observed simultaneously.

It is important to note that there can be certain conditions that can still prevent the system from achieving full observability depending on the trajectory of robot and the relative configuration of observed known landmarks. This can be explained using the following example. According to the usual notation, let the robot pose be denoted by $\mathbf{X}(k) = \begin{bmatrix} x(k) & y(k) & \theta(k) \end{bmatrix}^T$. Assume that the exteroceptive sensor on the robot (at location $\mathbf{V} \equiv (x, y)$) is observing two known landmarks denoted by $\mathbf{LM}_1 \equiv (x_1, y_1)$ and $\mathbf{LM}_2 \equiv (x_2, y_2)$, where x_1, y_1 and x_2, y_2 are the coordinate pairs of the two known landmarks. Assuming the vehicle location and the exteroceptive sensor coordinates coincide, the measurement Jacobian, $\mathbf{H}$, when observing both the landmarks simultaneously, can be expressed as,

$$\mathbf{H} = \begin{bmatrix} \Delta x_1/\Delta r_1 & \Delta y_1/\Delta r_1 & 0 & 0 & 0 & 1 & 0 \\ -\Delta y_1/(\Delta r_1)^2 & -\Delta x_1/(\Delta r_1)^2 & -1 & 0 & 0 & 0 & 1 \\ \Delta x_2/\Delta r_2 & \Delta y_2/\Delta r_2 & 0 & 0 & 0 & 1 & 0 \\ -\Delta y_2/(\Delta r_2)^2 & -\Delta x_2/(\Delta r_2)^2 & -1 & 0 & 0 & 0 & 1 \end{bmatrix} \tag{69}$$

where $\Delta x_i = x(k|k-1) - x_i$, $\Delta y_i = y(k|k-1) - y_i$, $\Delta r_i = \sqrt{(\Delta x_i)^2 + (\Delta y_i)^2}$ and i is an integer specifying the landmark being observed. Thus it can be established that when the first and the third rows or the second and the fourth rows of $\mathbf{H}$ are equivalent, the observability matrix of the system for this particular linearization is rank deficient. The conditions for the linearly dependent rows in $\mathbf{H}$ can thus be derived from (69) as

$$\Delta x_1/\Delta x_2 = \Delta y_1/\Delta y_2 = \Delta r_1/\Delta r_2, \tag{70}$$

$$\Delta x_1/\Delta x_2 = \Delta y_1/\Delta y_2 = \left(\Delta r_1/\Delta r_2\right)^2. \tag{71}$$

The conditions stipulated by eq. (70) or (71) occur when the vehicle position and the landmark locations are on a straight line. Thus, eq. (70) or (71) establishes that when the vehicle and the two landmarks being observed are on a straight line the problem of joint estimation of sensor biases (of both exteroceptive and proprioceptive sensors) and the vehicle state in MAL is unobservable. Let $\Delta x_i = x_i(k-1)$ and $\Delta y_i = y_i(k-1)$ be the x and y coordinates of the i^{th} (where i is any positive integer) landmark being observed, then from the measurement Jacobian $\mathbf{H}$ (which can be generalized to more than two landmarks in the same manner as eq. (69)) we can obtain the expression for linear dependency as:

$$\Delta x_1/\Delta y_1 = \Delta x_2/\Delta y_2 = \Delta x_3/\Delta y_3 = \cdots = \Delta x_n/\Delta y_n. \tag{72}$$

As stated, the condition stipulated by (70) and (71) occurs when the vehicle and all the landmarks being observed are on a straight line. Similarly, the condition (72) stipulates that all observed landmarks and the vehicle are on a straight line. This demonstrates that even though more than two landmarks are simultaneously observed, under the condition of (72), the observability matrix is still rank deficient. This is an important result, which states that the landmarks need to be observed in a manner that does not violate the conditions for observability. Thus it is always desirable to observe as many landmarks as possible so that at least two landmarks are not on a straight line with the vehicle location simultaneously in order to retain the full observability.

3.4. Rates of Convergence of Uncertainties

From the perspective of practical implementation it is important to know the rates of convergence of the estimated bias parameters of the estimation algorithm. The phenomenon of convergence can be better elucidated by studying the 1D MAL problem introduced in Section 1.2 using (14) together with the modified observability matrix of (68) that ensures full observability.

By employing continuous time equivalents of (14) and (68) it is possible to obtain a closed form solution for the uncertainty terms of the bias estimates and the vehicle location estimate. The factors that affect the rates of convergence of these uncertainties are clearly visible from the closed form solution. The continuous time process model, of the discrete time model (14) is:

$$\begin{bmatrix} \dot{x}_v(t) \\ \dot{u}_b(t) \\ \dot{s}_b(t) \end{bmatrix} = \begin{bmatrix} 0 & 1 & 0 \\ 0 & 0 & 0 \\ 0 & 0 & 0 \end{bmatrix} \begin{bmatrix} x_v(t) \\ u_b(t) \\ s_b(t) \end{bmatrix} + \begin{bmatrix} 1 \\ 0 \\ 0 \end{bmatrix} [u(t) + v(t)] \tag{73}$$

where $x_v(t)$ is the position of the robot, $u_b(t)$ is the bias of the proprioceptive sensor, $s_b(t)$ is the bias of the exteroceptive sensor, $u(t)$ is the proprioceptive sensor measurement at time t and $v(t) \sim N(0, q^2)$ represents the proprioceptive sensor noise and modeling uncertainties, if any. The analogous continuous time state vector of the problem is given by $\mathbf{X}(t) = \begin{bmatrix} x_v(t) & u_b(t) & s_b(t) \end{bmatrix}^T$ and the observation model incorporating an external sensor measurement when observing n landmarks is given by:

$$\mathbf{z}(t) = \mathbf{H}\mathbf{X}(t) + [\mathbf{L}^T \; 0]^T + \mathbf{w}(t) \tag{74}$$

where $\mathbf{w}(t) \sim N(\mathbf{0}_{(n+1)\times 1}, \mathbf{R})$ is the measurement noise, $\mathbf{R} = diag(r^2, r^2, \ldots, r^2, r_e^2)$ is the covariance matrix of $\mathbf{w}(t)$, r^2 is the variance of $\mathbf{w}(t)$, r_e^2 is the variance of the absolute sensor measurement noise, $\mathbf{L}$ is the vector of n known 1D landmarks stored in the map and $\mathbf{H}$ is given by (68). Let $\mathbf{P}(0) = diag(0, \sigma_{bu}^2, \sigma_{bs}^2)$ be the initial error covariance matrix $\mathbf{P}(t)$ (model (73)) of $\mathbf{X}(t)$, $\mathbf{I}$ be the identity matrix of size 3×3

and σ_{bu}^2 and σ_{bs}^2 denote the initial variances of the proprioceptive and exteroceptive sensor biases. The initial uncertainty of the vehicle is assumed to be zero. Then $\mathbf{P}(t)$ is governed by the continuous time Riccati equation:

$$\dot{\mathbf{P}}(t) = \mathbf{F}\mathbf{P}(t) + \mathbf{P}(t)\mathbf{F}^{\mathbf{T}} + \mathbf{G}\mathbf{Q}\mathbf{G}^{\mathbf{T}} - \mathbf{P}(t)\mathbf{H}^{\mathbf{T}}\mathbf{R}^{-1}\mathbf{H}\mathbf{P}(t) \tag{75}$$

where $\mathbf{G} = \begin{bmatrix} 1 & 0 & 0 \end{bmatrix}^T$ and $\mathbf{F} = \begin{bmatrix} [0\ 1\ 0]^T & \mathbf{0}_{3\times 2} \end{bmatrix}^T$. The solution to this Riccati equation (Brown and Hwang 1992) is of the form $\mathbf{P}(t) = \mathbf{M}(t)\mathbf{N}^{-1}(t)$, where $\mathbf{M}(t)$ and $\mathbf{N}(t)$ are as follows:

$$\begin{bmatrix} \dot{\mathbf{M}}(t) \\ \dot{\mathbf{N}}(t) \end{bmatrix} = \begin{bmatrix} \mathbf{F} & \mathbf{G}\mathbf{Q}\mathbf{G}^{\mathbf{T}} \\ \mathbf{H}^{\mathbf{T}}\mathbf{R}^{-1}\mathbf{H} & -\mathbf{F}^{\mathbf{T}} \end{bmatrix} \begin{bmatrix} \mathbf{M}(t) \\ \mathbf{N}(t) \end{bmatrix}, \tag{76}$$

$$\begin{bmatrix} \mathbf{M}(0) \\ \mathbf{N}(0) \end{bmatrix} = \begin{bmatrix} \mathbf{P}(0) \\ \mathbf{I} \end{bmatrix}. \tag{77}$$

Then the characteristic equation $\mathbf{C}(t)$ of the system, and the i^{th} row and j^{th} column element $\mathbf{P}(i, j)$ of $\mathbf{P}(t)$ for all i and j can be obtained by solving (76) and (77) as follows:

$$\begin{aligned}\mathbf{C}(t) = {} & \left(nr_e^2 + r^2\right)(nq^2r^2\sigma_{bu}^2\sigma_{bs}^2(1 - e^{-\alpha t})^2t^2 \\ & + ((\sigma_{bu}^2(nr_e^2 + r^2) + nq^2\sigma_{bs}^2)(1 + e^{-2\alpha t})q^2r^2 \\ & + nr^2r_e^2\sigma_{bu}^2\sigma_{bs}^2\alpha(1 - e^{-2\alpha t}))t) \\ & + q^4r^2(nr_e^2 + r^2)(1 + e^{-2\alpha t}) \\ & - 2n^2r_e^4r^2\sigma_{bu}^2\sigma_{bs}^2(1 - e^{-\alpha t})^2 \\ & + r^2r_e^2\alpha(n^2r_e^2q^2\sigma_{bs}^2 \\ & - r^2\sigma_{bu}^2(nr_e^2 + r^2))((1 - e^{-2\alpha t})),\end{aligned} \tag{78}$$

$$\begin{aligned}\mathbf{P}(1, 1) = {} & \left(1/\mathbf{C}(t)\right)(2n^2r_e^4\sigma_{bs}^2(1 - e^{-\alpha t})^2 \\ & + r^2r_e^2\alpha(nr_e^2 + r^2 + n\sigma_{bs}^2t)(1 - e^{-2\alpha t})) \\ & (q^2 + \sigma_{bu}^2t)q^2r^2,\end{aligned} \tag{79}$$

$$\begin{aligned}\mathbf{P}(1, 2) = {} & \left(1/\mathbf{C}(t)\right)(2n^2r_e^4\sigma_{bs}^2(1 - e^{-\alpha t})^2 \\ & + r^2r_e^2\alpha(nr_e^2 + r^2 + n\sigma_{bs}^2t)(1 - e^{-2\alpha t}))\sigma_{bu}^2q^2r^2,\end{aligned} \tag{80}$$

$$\begin{aligned}\mathbf{P}(1, 3) = {} & \left(1/\mathbf{C}(t)\right)(1 - e^{-\alpha t})^2r^2r_e^2q^2(nr_e^2 + r^2) \\ & (q^2 + \sigma_{bu}^2t)n\sigma_{bs}^2,\end{aligned} \tag{81}$$

$$\begin{aligned}\mathbf{P}(2, 2) = {} & \left(1/\mathbf{C}(t)\right)(r^2q^2(nr_e^2 + r^2)(1 + e^{-2\alpha t}) \\ & (nr_e^2 + r^2 + n\sigma_{bs}^2t) + n^2r_e^4r^2\alpha(1 - e^{-2\alpha t}))q^2\sigma_{bu}^2,\end{aligned} \tag{82}$$

$$\mathbf{P}(2, 3) = \left(1/\mathbf{C}(t)\right)\sigma_{bu}^2\sigma_{bs}^2q^2r^2r_e^2n(nr_e^2 + r^2)(1 - e^{-\alpha t})^2, \tag{83}$$

$$\begin{aligned}\mathbf{P}(3, 3) = {} & \left(1/\mathbf{C}(t)\right) \\ & (q^2(nr_e^2 + r^2)(1 + e^{-2\alpha t})(q^2 + \sigma_{bu}^2t) \\ & - r^2r_e^2\alpha\sigma_{bu}^2(1 - e^{-2\alpha t}))\sigma_{bs}^2(nr_e^2 + r^2)r^2,\end{aligned} \tag{84}$$

$$\alpha = (q/(rr_e))\left(nr_e^2 + r^2\right)^{0.5}. \tag{85}$$

Here, $1/\alpha$ is the time constant of the decay of the covariance terms. All the other terms of the covariance matrix can be derived from (78) to (85) using the symmetry of $\mathbf{P}(t)$. The eqs (78) to (85) show that the error covariance terms of $\mathbf{X}(t)$ decay exponentially initially at a time constant of $1/\alpha$ and then converge asymptotically to the steady state covariance according to the expressions (78) to (85). This asymptotic convergence of the error covariance terms can be a disadvantage in actual practice. It may be interesting to note that this convergence rate is not affected by the biases or their initial uncertainties and depends only on the proprioceptive and exteroceptive sensor noise terms, absolute sensor measurement noise term and the number of known landmarks in the stored map. When the variance of the absolute sensor noise r_e^2 is very large compared to r^2 (i.e., the landmark based information dominates the external sensor based information) the time constant approaches $\sqrt{r^2/(nq^2)}$. In other words, the smaller the ratio between exteroceptive sensor noise and the process noise (proprioceptive sensor noise and the modeling uncertainty) or the larger the number of landmarks observed simultaneously, the faster will be the convergence of the state variances to their steady state values. The steady state covariance of $\mathbf{X}(t)$, $\mathbf{P}(\infty)$ can be obtained from (78) to (85) by taking the limit as $t \to \infty$. Thus it can be seen that all the state covariance terms, except that of the vehicle position, approach zero. The vehicle position variance approaches q^2/α.

Thus we can conclude that the rates of convergence of the state uncertainties do not depend on the bias parameters or their initial uncertainties. They depend only on proprioceptive and exteroceptive sensor noise and the modeling uncertainty. These theoretically established properties provide useful insight into the problem and are useful in practical applications.

4. Simulations and Experiments

4.1. Simulation of Standard 2D MAL

In this section we consider relevant simulation scenarios to establish the importance of jointly estimating the biases and the vehicle state online and also to verify the theoretical findings on the observability, convergence and lower bounds in the context of MAL.

The performance of the algorithm for the joint estimation of the sensor biases and the vehicle state in MAL is initially evaluated in a simulated 2D planar environment consisting of 25 point landmarks. It is assumed that the vehicle is equipped with wheel encoders (proprioceptive sensors) and a laser range-bearing sensor (exteroceptive sensor), such as a SICK LMS 290 laser measurement system, and is traveling in an approximately circular path of radius 20 m.

The process and observation models and joint bias and vehicle state estimation formulae for this 2D MAL simulation are given by equations (16) to (25). The simulated values of the bias parameters of the sensors are: LMS range bias of 0.5 m, angle bias of 2°, speed sensor input bias of 0.25 m/s and steering input angle sensor bias of 1° and random noise sequences with variances 0, 0, 0.0004 m^2/s^4 and $4 \times 10^{-6} rad^2/s^2$ respectively. The update rate of all sensors is 10 Hz.

At the outset, it is important to state that when there are biases in the sensors and no bias estimation is utilized it is almost impossible to estimate the vehicle pose consistently. Figures 2(a) to (h) show simulation results of MAL with the online joint estimation and correction of biases. The results clearly show that MAL works well with the online joint sensor bias estimation with ever diminishing uncertainties of the bias estimates, as established in the theoretical discussion in Section 3.1. The graphs in Figures 2(g) and (h) also show that the uncertainties of the bias estimates reach a lower bound. In particular, the convergence of the estimated bias parameters to the actual values establish that in the 2D MAL case, observing two or more landmarks makes the system fully observable as established in Section 3.3, obviating the need for any absolute sensor such as a GPS. Figure 3 shows the average value of the normalized estimation error squared (NEES) at each time step, for a 100 run, Monte-Carlo simulation. As the sample average is within the 95% confidence region with the expected probability, it can be concluded that the estimator is consistent.

4.2. Use of Inertial Sensors in MAL

The application of online bias estimation is most important when using inertial sensors in MAL. With the advent of low cost (strap down) inertial sensors, use of inertial sensor suites in many autonomous underwater and land navigation systems has become economically viable. These sensor suites are essential in field robotics where extensive uneven terrain has to be explored and mapped. The ability to navigate in 3D terrain and the fact that the localization solution can be obtained independently of vehicle's kinematic model are some of the benefits of using inertial sensors in MAL. However, the major disadvantage of inertial sensor suites especially the low cost strap down variety, is their inherent sensor biases, drifts and scale factors. Random walks and time varying biases present in gyros (angular rate) and acceleration inertial sensors (Grewal, Weill, and Andrews 2001), cause the offline calibration methods to be less effective.

We demonstrate how the theoretical results, discussion and the principles given in Section 3 can be extended for the case of joint online estimation of biases in inertial sensors used for MAL. The autonomous vehicle used is shown in Figure 4. To keep the explanations and derivations simple it is assumed that the vehicle is moving on a flat horizontal planar surface and that the inertial sensor assembly is mounted at or near the center of gravity (COG) of the vehicle.

The vehicle motion is referenced to a global coordinate frame, which is the earth reference frame or the navigation frame **{n}** forming a right handed orthogonal set of axes NED (North, East and Down) as shown in Figure 5. The vehicle body reference frame **{v}** has its origin at the COG of the vehicle with its X-axis in the direction of heading and the Y-axis and Z-axis as shown in the Figure 5. The proprioceptive sensor or the inertial measurement unit's (IMU) coordinate frame is coincident with the vehicle frame $\{\mathbf{v}\}$. The vehicle's orientation (i.e., orientation of vehicle body frame $\{\mathbf{v}\}$) is therefore represented using the three Euler angles ϕ (rotation about vehicle X axis or roll), θ (rotation about vehicle Y axis or pitch) and ψ (rotation about vehicle Z axis or yaw) as shown in Figure 5. Now if the vehicle is confined to move on a flat horizontal plane and its position in X and Y coordinates and velocities in the X, Y and Z directions, with respect to the global navigation frame $\{\mathbf{n}\}$, are $x_v^{\mathbf{n}}$, $y_v^{\mathbf{n}}$, $v_x^{\mathbf{n}}$, $v_y^{\mathbf{n}}$ and $v_z^{\mathbf{n}}$ respectively, then the whole process state $\mathbf{x}(k)$ incorporating the vehicle state $\mathbf{x}_v(k)$ and the biases in the inertial sensor is:

$$\begin{aligned}
\mathbf{x}(k) &= \begin{bmatrix} \mathbf{x}_{\mathbf{v}}^T(k) & (\mathbf{b}^{\mathbf{v}}(k))^T \end{bmatrix}^T \\
\mathbf{x}_v(k) &= \begin{bmatrix} x_v^{\mathbf{n}} & y_v^{\mathbf{n}} & v_x^{\mathbf{n}} & v_y^{\mathbf{n}} & v_z^{\mathbf{n}} & \phi & \theta & \psi \end{bmatrix}^T \\
\mathbf{b}^{\mathbf{v}}(k) &= \begin{bmatrix} b_{x_a}^{\mathbf{v}}(k) & b_{y_a}^{\mathbf{v}}(k) & b_{z_a}^{\mathbf{v}}(k) & b_{x_\omega}^{\mathbf{v}}(k) & b_{y_\omega}^{\mathbf{v}}(k) & b_{z_\omega}^{\mathbf{v}}(k) \end{bmatrix}^T
\end{aligned} \tag{86}$$

where $\mathbf{b}^{\mathbf{v}}(k)$ is the vector of biases of the IMU and its elements $b_{x_a}^{\mathbf{v}}$, $b_{y_a}^{\mathbf{v}}$, $b_{z_a}^{\mathbf{v}}$, $b_{x_\omega}^{\mathbf{v}}$, $b_{y_\omega}^{\mathbf{v}}$ and $b_{z_\omega}^{\mathbf{v}}$ represent the biases in the linear acceleration measurements ($a_x^{\mathbf{v}}$, $a_y^{\mathbf{v}}$ and $a_z^{\mathbf{v}}$) and the angular velocity measurements ($\omega_x^{\mathbf{v}}$, $\omega_y^{\mathbf{v}}$ and $\omega_z^{\mathbf{v}}$) with respect to the vehicle body frame $\{\mathbf{v}\}$. Let $\eta_{x_a}^{\mathbf{v}}$, $\eta_{y_a}^{\mathbf{v}}$, $\eta_{z_a}^{\mathbf{v}}$, $\eta_{x_\omega}^{\mathbf{v}}$, $\eta_{y_\omega}^{\mathbf{v}}$ and $\eta_{z_\omega}^{\mathbf{v}}$ denote the assumed temporally uncorrelated noise terms of the measurements $a_x^{\mathbf{v}}$, $a_y^{\mathbf{v}}$, $a_z^{\mathbf{v}}$, $\omega_x^{\mathbf{v}}$, $\omega_y^{\mathbf{v}}$ and $\omega_z^{\mathbf{v}}$respectively. Let $\eta_x^{\mathbf{n}}$ and $\eta_y^{\mathbf{n}}$ represent the modeling uncertainties of the vehicle's (x, y) position with reference to the navigation frame $\{\mathbf{n}\}$. We assume that the vehicle state and the bias state evolve as follows:

$$\begin{bmatrix} x_v^{\mathbf{n}}(k) \\ y_v^{\mathbf{n}}(k) \end{bmatrix} = \begin{bmatrix} x_v^{\mathbf{n}}(k-1) + \Delta t v_x^{\mathbf{n}}(k-1) \\ y_v^{\mathbf{n}}(k-1) + \Delta t v_y^{\mathbf{n}}(k-1) \end{bmatrix} + \begin{bmatrix} \eta_x^{\mathbf{n}} \\ \eta_y^{\mathbf{n}} \end{bmatrix}, \tag{87}$$

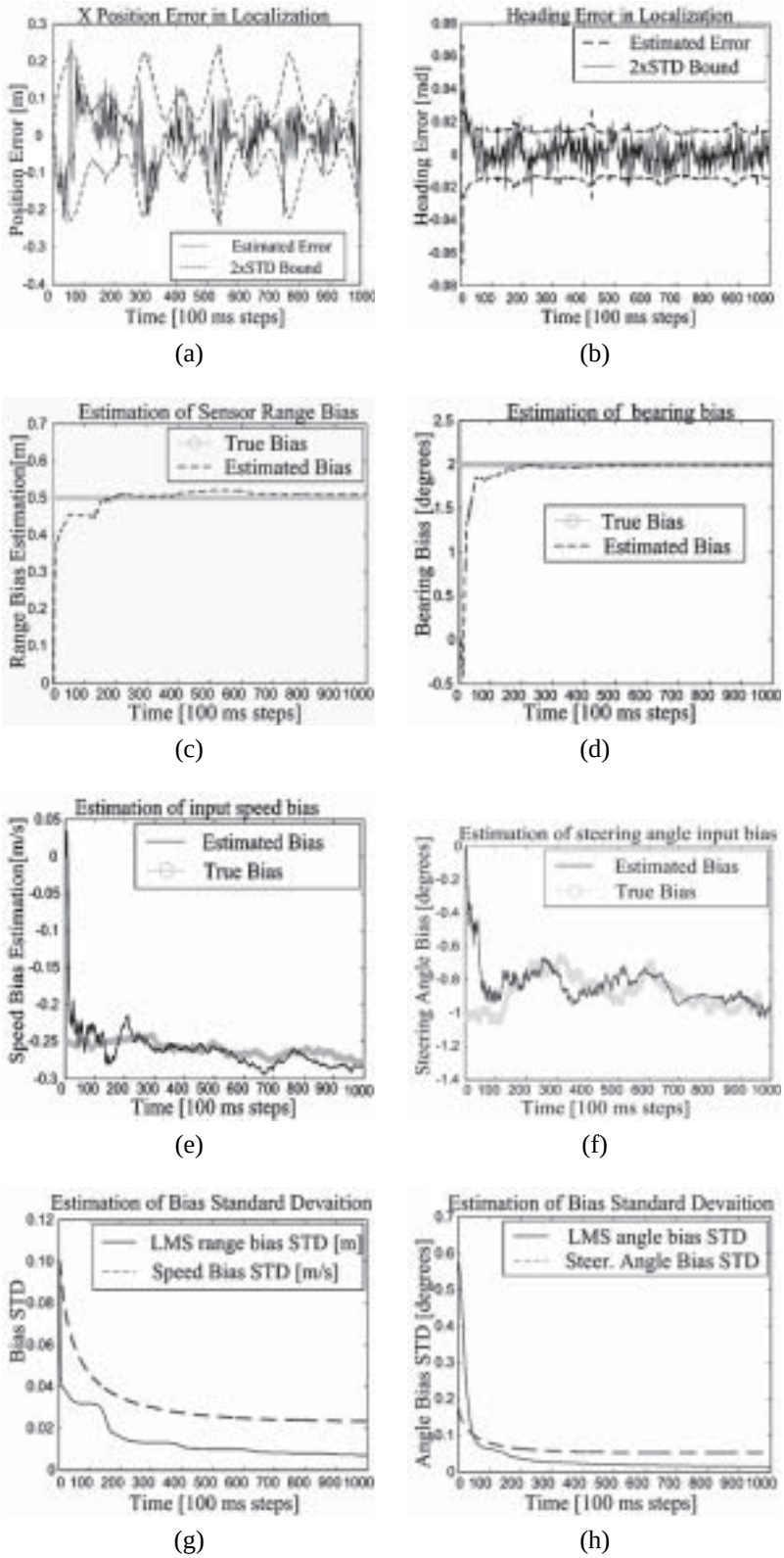

Fig. 2. Graphs (a) and (b) show the 2D MAL, localization error in x and heading with online bias estimation. Graphs (c), (d), (e) and (f) show sensor bias estimates. Graphs (g) and (h) show the variation of the standard deviation of the sensor biases.

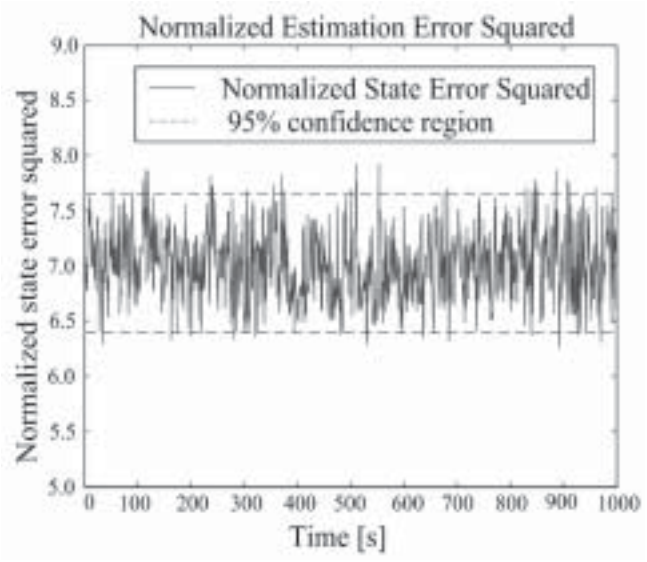

Fig. 3. The sample average values of the NEES for a 100 run Monte-Carlo simulation in 2D MAL. The dotted lines show the 95% confidence regions.

Fig. 4. The autonomous vehicle used in MAL experiments.

$$\begin{bmatrix} v_x^{\mathbf{n}}(k) \\ v_y^{\mathbf{n}}(k) \\ v_z^{\mathbf{n}}(k) \end{bmatrix} = \begin{bmatrix} v_x^{\mathbf{n}}(k-1) \\ v_y^{\mathbf{n}}(k-1) \\ v_z^{\mathbf{n}}(k-1) \end{bmatrix} + \left(\mathbf{C_{vn}} \begin{bmatrix} a_x^{\mathbf{v}} + b_{x_a}^{\mathbf{v}}(k-1) + \eta_{x_a}^{\mathbf{v}} \\ a_y^{\mathbf{v}} + b_{y_a}^{\mathbf{v}}(k-1) + \eta_{y_a}^{\mathbf{v}} \\ a_z^{\mathbf{v}} + b_{z_a}^{\mathbf{v}}(k-1) + \eta_{z_a}^{\mathbf{v}} \end{bmatrix} - \begin{bmatrix} 0 \\ 0 \\ g \end{bmatrix} \right) \Delta t, \tag{88}$$

$$\begin{aligned} \phi(k) = \phi(k-1) &+ ((\omega_x^{\mathbf{v}} + b_{x_\omega}^{\mathbf{v}}(k-1) + \eta_{x_\omega}^{\mathbf{v}}) \\ &+ ((\omega_y^{\mathbf{v}} + b_{y_\omega}^{\mathbf{v}}(k-1) + \eta_{y_\omega}^{\mathbf{v}})(\sin\phi(k-1)) \\ &+ (\omega_z^{\mathbf{v}} + b_{z_\omega}^{\mathbf{v}}(k-1) + \eta_{z_\omega}^{\mathbf{v}})\cos(\phi(k-1))) \\ &\tan(\theta(k-1)))\Delta t, \end{aligned} \tag{89}$$

$$\begin{aligned} \theta(k) = \theta(k-1) &+ ((\omega_y^{\mathbf{v}} + b_{y_\omega}^{\mathbf{v}}(k-1) + \eta_{y_\omega}^{\mathbf{v}})\cos(\phi(k-1)) \\ &- (\omega_z^{\mathbf{v}} + b_{z_\omega}^{\mathbf{v}}(k-1) + \eta_{z_\omega}^{\mathbf{v}})\sin(\phi(k-1)))\Delta t, \end{aligned} \tag{90}$$

$$\begin{aligned} \psi(k) = \psi(k-1) &+ ((\omega_y^{\mathbf{v}} + b_{y_\omega}^{\mathbf{v}}(k-1) + \eta_{y_\omega}^{\mathbf{v}}) \\ &\sin(\phi(k-1))\sec(\theta(k-1)))\Delta t \\ &+ ((\omega_z^{\mathbf{v}} + b_{z_\omega}^{\mathbf{v}}(k-1) + \eta_{z_\omega}^{\mathbf{v}})\cos(\phi(k-1)) \\ &\sec(\theta(k-1)))\Delta t, \end{aligned} \tag{91}$$

$$\mathbf{b}^{\mathbf{v}}(k) = \mathbf{A}_b\mathbf{b}^{\mathbf{v}}(k-1) + \mathbf{c}_b^{\mathbf{v}} + \boldsymbol{\eta}_b^{\mathbf{v}}, \tag{92}$$

$$\mathbf{C_{vn}} = \begin{bmatrix} C_\theta C_\psi & -C_\phi S_\psi + S_\phi S_\theta C_\psi & S_\phi S_\psi + C_\phi S_\theta C_\psi \\ C_\theta S_\psi & C_\phi C_\psi + S_\phi S_\theta S_\psi & -S_\phi C_\psi + C_\phi S_\theta S_\psi \\ -S_\theta & S_\phi C_\theta & C_\phi C_\theta \end{bmatrix}. \tag{93}$$

Here Δt is the sampling time of the inertial sensor, g is the gravitational constant, $\mathbf{C_{vn}}$ is the rotational matrix describing the orientation of the vehicle frame **{v}** with respect to the navigation frame **{n}**, and $C_x = \cos(x)$ and $S_x = \sin(x)$ for $x \in \{\phi,\ \theta,\ \psi\}$. $\mathbf{A}_b$ is a 6×6 diagonal matrix, $\mathbf{c}_b^{\mathbf{v}}$ is a 6×1 constant vector and $\boldsymbol{\eta}_b^{\mathbf{v}}$ is a 6×1 temporally uncorrelated noise vector with covariance $\mathbf{Q}_b$ (diagonal matrix). The values of $\mathbf{A}_b$, $\mathbf{c}_b^{\mathbf{v}}$ and $\mathbf{Q}_b$ can be experimentally determined. To account for the offsets and drifts in the bias phenomena of inertial sensors, they are modeled as given by (92). Equation (92) is able to accommodate exponential variation (Barshan and Durrant-Whyte 1995) of biases or a constant but unknown component and a random walk component (Grewal, Weill, and Andrews 2001). The error models of the gyroscopes and the accelerometers are given by (94) and (95):

$$\boldsymbol{\omega}_{i/p} = \mathbf{M}_{gyro}\left(\boldsymbol{\omega}_{o/p} + \boldsymbol{\omega}_{bias}\right) + \boldsymbol{\eta}_\omega, \tag{94}$$

$$\mathbf{a}_{i/p} = \mathbf{M}_{acc}\left(\mathbf{a}_{o/p} + \mathbf{a}_{bias}\right) + \boldsymbol{\eta}_a, \tag{95}$$

where $\boldsymbol{\omega}_{i/p}$ is the actual input rotational rate vector, $\boldsymbol{\omega}_{o/p}$ is the measured rotational rate vector $\left[\omega_x^{\mathbf{v}},\ \omega_y^{\mathbf{v}}, \omega_z^{\mathbf{v}}\right]^T$, $\boldsymbol{\omega}_{bias}$ is the three axis gyro bias vector $\left[b_{x_\omega}^{\mathbf{v}}\ b_{y_\omega}^{\mathbf{v}}\ b_{z_\omega}^{\mathbf{v}}\right]^T$, $\boldsymbol{\eta}_\omega$ is the gyroscope measurement noise vector $\left[\eta_{x_\omega}^{\mathbf{v}},\ \eta_{y_\omega}^{\mathbf{v}}, \eta_{z_\omega}^{\mathbf{v}}\right]^T$, $\mathbf{a}_{i/p}$ is the

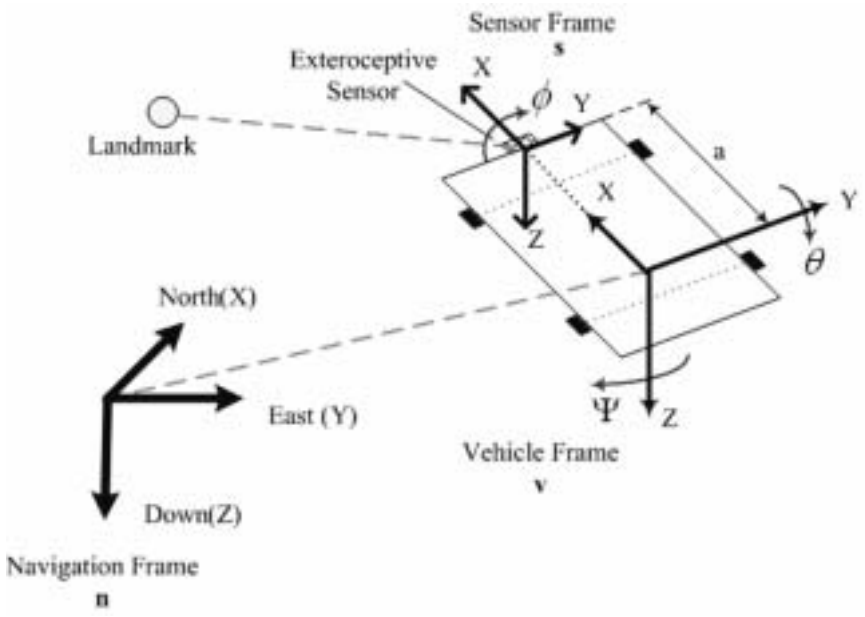

Fig. 5. Reference coordinate frames.

actual input acceleration vector, $\mathbf{a}_{o/p}$ is the measured acceleration vector $\left[a_x^{\mathbf{v}},\ a_y^{\mathbf{v}}, a_z^{\mathbf{v}}\right]^T$, $\mathbf{a}_{bias}$ is the acceleration bias vector $\left[b_{x_a}^{\mathbf{v}}\ b_{y_a}^{\mathbf{v}}\ b_{z_a}^{\mathbf{v}}\right]^T$, and $\boldsymbol{\eta}_a$ is the accelerometer measurement noise vector $\left[\eta_{x_a}^{\mathbf{v}},\ \eta_{y_a}^{\mathbf{v}},\ \eta_{z_a}^{\mathbf{v}}\right]^T$. $\mathbf{M}_{gyro}$ and $\mathbf{M}_{acc}$ are 3×3 matrices used for scale factor and misalignment compensation of the gyroscopes. The scale factor matrices are assumed to be identity matrices. Now the complete process model of the system can be expressed as:

$$\mathbf{x}(k) = \mathbf{f}(\mathbf{x}_v(k-1), \mathbf{u}^{\mathbf{v}}(k-1), \mathbf{b}^{\mathbf{v}}(k-1), \boldsymbol{\eta}(k-1)) \quad (96)$$

where $\mathbf{u}^{\mathbf{v}}(k-1) = [a_x^{\mathbf{v}}\ a_y^{\mathbf{v}}\ a_z^{\mathbf{v}}\ \omega_x^{\mathbf{v}}\ \omega_y^{\mathbf{v}}\ \omega_z^{\mathbf{v}}]$ and $\mathbf{f}(.)$ is given by the concatenated right hand sides of the equations (87) to (92) and $\boldsymbol{\eta}$ is a zero mean process noise sequence.

The covariance $\mathbf{Q}(k)$ representing the entire noise characteristics of the measurements and biases of the IMU is given by:

$$\mathbf{Q(k)} = \left(\frac{\partial \mathbf{f}}{\partial \mathbf{u}^{\mathbf{v}}}\right)\mathbf{Q_u}\left(\frac{\partial \mathbf{f}}{\partial \mathbf{u}^{\mathbf{v}}}\right)^T + \begin{bmatrix} \mathbf{Q_{xy}} & \mathbf{0}_{2\times6} & \mathbf{0}_{2\times6} \\ \mathbf{0}_{6\times2} & \mathbf{0}_{6\times6} & \mathbf{0}_{6\times6} \\ \mathbf{0}_{6\times2} & \mathbf{0}_{6\times6} & \mathbf{Q}_b \end{bmatrix} \quad (97)$$

where $\mathbf{Q_u}$ and $\mathbf{Q_{xy}}$ are zero mean diagonal noise covariance matrices of the concatenated IMU measurement noise vector, $[\eta_{x_a}^{\mathbf{v}}\ \eta_{y_a}^{\mathbf{v}}\ \eta_{z_a}^{\mathbf{v}}\ \eta_{y_\omega}^{\mathbf{v}}\ \eta_{y_\omega}^{\mathbf{v}}\ \eta_{y_\omega}^{\mathbf{v}}]^T$ and the vector representing the modeling uncertainty $[\eta_x^{\mathbf{n}}\ \eta_y^{\mathbf{n}}]^T$ respectively.

In the following, the observation model is determined for the case of a vehicle moving on a horizontal plane whilst making measurements to point landmarks. It is assumed that the features, or landmarks are observed using an onboard exteroceptive sensor, such as a 2D range-bearing sensor. As shown in Figure 5, the exteroceptive sensor's frame **{s}** is assumed to be aligned but not coincident with the vehicle frame **{v}.** Let $\mathbf{x}_s^{\mathbf{v}}$ represent the exteroceptive sensor's position in the vehicle frame **{v}**, $\mathbf{x}_s^{\mathbf{n}}$ the exteroceptive sensor's position in the navigation frame **{n}**, and $\mathbf{x}_v^{\mathbf{n}}$ the vehicle's coordinates in the navigation frame **{n}.** Let $\mathbf{x}_L^{\mathbf{n}}$ represent the coordinates of a point landmark in **{n}**, and $\mathbf{x}_L^{\mathbf{s}} = \begin{bmatrix} L_x & L_y & L_z \end{bmatrix}^T$ its coordinates in the exteroceptive sensor's frame **{s}.** Since it is assumed that the vehicle moves on a flat horizontal plane whose elevation is known, the z coordinates of the position vectors $\mathbf{x}_s^{\mathbf{v}}, \mathbf{x}_s^{\mathbf{n}}, \mathbf{x}_v^{\mathbf{n}}$, and $\mathbf{x}_L^{\mathbf{s}}$ are known a priori. Since $\mathbf{C_{vn}}$ is the relative orientation between **{v}** and **{n}**, and there is no relative orientation between **{v}**, and **{s},** we have

$$\mathbf{x}_s^{\mathbf{n}} = \mathbf{x}_v^{\mathbf{n}} + \mathbf{C_{vn}}\mathbf{x}_s^{\mathbf{v}}, \quad \mathbf{x}_L^{\mathbf{s}} = (\mathbf{C_{vn}})^T(\mathbf{x}_L^{\mathbf{n}} - \mathbf{x}_s^{\mathbf{n}}). \quad (98)$$

Now, it is straightforward to show that the observation model for a single landmark observation from the range-bearing sensor is,

$$\mathbf{z}(k) = \begin{bmatrix} \sqrt{L_x^2 + L_y^2} \\ \tan^{-1}\left(L_y / L_x\right) + \pi/2 \end{bmatrix}. \quad (99)$$

The observation model of (99) can be easily generalized to any number of landmarks by concatenating the observation vector with the relative measurements to the landmarks.

The prediction and update equations of MAL are similar to (7) to (13). Since the vehicle is assumed to be moving on a horizontal plane and there is no side slip, the vehicle

motion in the X and Y axis in its frame**{v}** will be zero. These nonholonomic constraints (i.e., $v_y^{\mathbf{v}} = 0$, and $v_z^{\mathbf{v}} = 0$) are also used as virtual observations in the joint online bias estimation process (Koifman and Bar-Itzhack 1999; Bingbing and Adams 2005). Now the vehicle's velocity vector, referenced to its frame **{v}**, can be expressed as:

$$\left[v_x^{\mathbf{v}}\ v_y^{\mathbf{v}}\ v_z^{\mathbf{v}}\right]^T = (\mathbf{C_{vn}})^T \left[v_x^{\mathbf{n}}\ v_y^{\mathbf{n}}\ v_z^{\mathbf{n}}\right]^T, \tag{100}$$

$$v_y^{\mathbf{v}} = 0 + \eta_x \tag{101}$$

$$v_z^{\mathbf{v}} = 0 + \eta_z, \tag{102}$$

where η_x and η_z are Gaussian noise sequences, which model any violation of the nonholonomic constraints.

As discussed earlier, it makes sense to investigate the observability of the system in the presence of biases before any attempt is made to estimate the parameters online. In IMU aided MAL with joint estimation of inertial bias parameters and the vehicle state, there are in all 14 state variables in the system state; 8 describing the vehicle state, and 6 corresponding to the biases in the inertial sensor. Therefore, for complete observability of the vehicle states and inertial bias parameters the rank of the observability Grammian of the system ((86) to (102)) must be 14. The observability of the system ((86) to (102)) is investigated by symbolic manipulation with and without the imposition of the nonholonomic constraints and a varying number of landmarks in the MAL state vector. The symbolic analysis is verified through empirical runs of the joint bias and vehicle state MAL estimation algorithm. When the nonholonomic constraints ((100) to (102)) are not imposed the rank of the observability matrix is 9. However, when observing two landmarks (with corresponding change in the observation model (99)), the rank increases from 9 to 11. Increasing the observed landmarks to three and beyond only increases the rank to a maximum of 12. That is despite being able to observe more than three landmarks the observability Grammian still remains rank deficient by 2. As expected, in the given setting the required full rank of 14 is only achievable through the imposition of the nonholonomic constraints (as virtual observations) as there is no sensor providing information about the Z-dimension. Furthermore, close examination of the observability Grammian of the system when observing two landmarks reveals that there is little chance that equations such as (70) and (71) are satisfied simultaneously, which makes the system unobservable. This is because the number of conditions that must be simultaneously satisfied for the rows of the measurement Jacobian of (99) to be linearly dependent is larger than in the case of the measurement Jacobian (69) for standard 2D MAL with bias estimation.

It is important to note that given a 3D sensor, such as a 3D laser measurement system or a stereo vision system, it would be straightforward to incorporate the Z-dimension of the vehicle location coordinates and landmark coordinates in the formulation and hence, relax the assumption of a flat surface.

4.3. Simulation of IMU Aided MAL

The properties of the online bias estimation and correction problem in IMU aided MAL is studied by conducting simulations in a planar environment consisting of several point landmarks (Figure 6). The vehicle is assumed to make several rounds in an approximately elliptical path at a forward speed of approximately 4 m/s. As described in Section 4.2, a 2D range-bearing sensor and an IMU (three axis angular rate and linear acceleration measurements) are assumed to be onboard the vehicle. The gyro (rate sensor) and acceleration bias parameters in all three axes of the IMU are set to constant values of $1.5^0 s^{-1}$ and 12 mg respectively. The random walk components due to the biases in the gyro and accelerometer of the IMU are set to $4.5^0 \Big/ \sqrt{\text{hr}}$ and $0.1\ \text{ms}^{-1} \Big/ \sqrt{\text{hr}}$ respectively. The sampling rates of the range-bearing sensor and the IMU were set to 10 Hz and 50 Hz respectively.

Figures 7(a) and (b) show the localization error distributions of IMU aided MAL with online bias estimation. The results of the estimation of the bias parameters and their uncertainties in the IMU are shown in Figures 8 and 9. It can be seen that both localization errors and uncertainty (variance) in the biases are bounded by the 2σ limits demonstrating the filter's consistency. In general, it may be noted that the uncertainties or variances of the estimated bias parameters settle to a lower bound as predicted by the theory detailed in Section 3.2.

The random walk behavior in the biases and the intermittent unavailability of observations cause the uncertainty in the biases to increase at certain instances (Figures 8(a), (c), (e) and 9(a), (c) and (e)). For example, all but the uncertainty of

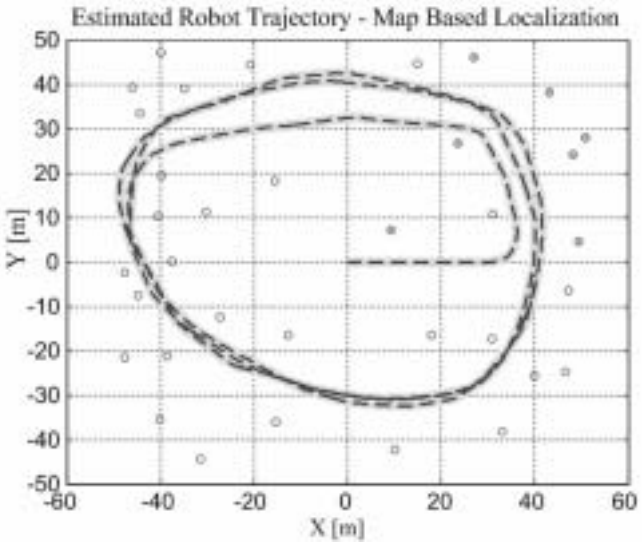

Fig. 6. IMU aided MAL simulation. The estimated path is shown by the darker dashed line and the true path is shown by the lighter solid line. The true landmarks and estimated landmarks are shown as circles and crosses respectively.

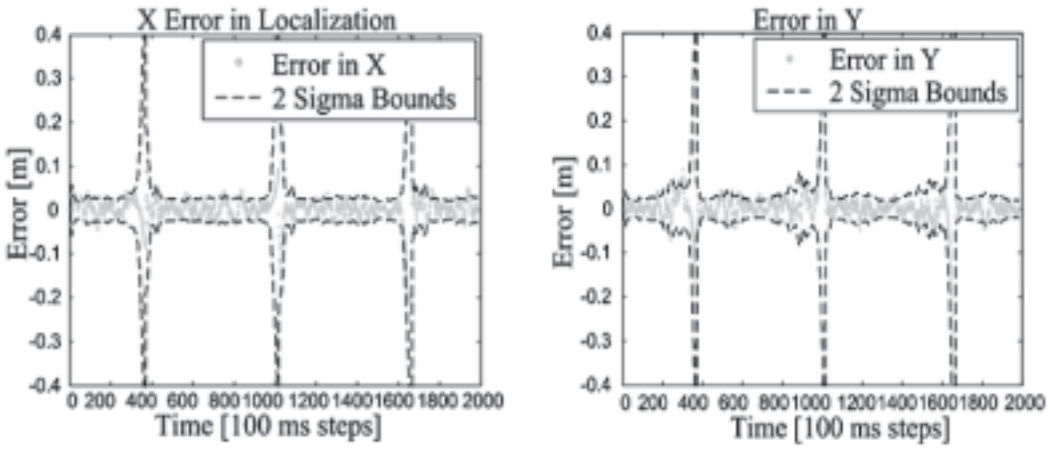

(a) (b)

Fig. 7. Localization errors of X, Y coordinates of vehicle in navigation frame in IMU aided MAL.

$b^{\mathrm{v}}_{z_a}(k)$, increase at time instances 40 s, 100 s, and 180 s due to inadequate landmark measurement updates at these times. The decrease in the uncertainty of $b^{\mathrm{v}}_{z_a}(k)$ is due mainly to information available via nonholonomic constraints (or virtual observations) at all times regardless of whether landmarks are observed or not. Figure 10 shows the average value of the normalized estimation error squared (NEES) at each time step for a 100 run Monte Carlo simulation of the IMU aided MAL. Since the state vector for IMU aided MAL with concurrent bias estimation described here consists of 14 states, the chi-square 95% confidence limits are 13.14 and 14.88. As the sample average is within the 95% confidence region with the expected probability, it follows that the estimator is consistent.

Figures 11, 12 and 13 show the results obtained assuming that the constant bias terms are known a priori, which in effect simulates the offline calibration and initialization of biased sensors. The parameters used in Section 4.2 to model the random walk behavior of biases are used in the simulations. It is noted that the estimation errors in the velocity (Figure 11) and location (Figure 12) diverge shortly after initialization. The rapid divergence of the errors is mainly a result of data association failures. Variations in the inertial biases cause measurements to fall outside the validation regions of predicted landmarks thus resulting in data association failures. Figure 13 shows the sample average of the normalized state estimation squared error plot for 50 Monte-Carlo runs. Since the full state vector excludes the constant bias terms (assumed known a priori through offline calibration), it has eight components. Hence, the chi-square 95% confidence limits are 5.22 and 6.83. It is observed that the sample average of NEES diverges from the 95% confidence region demonstrating the inconsistency of the filter.

Table 1 shows how the divergence rate is affected by the variations of biases due to increasing random walk behavior. It is however, assumed that the constant bias terms are known a priori. The results suggest that offline calibration, initialization and resetting can only be effective for short periods of time and for small variations in the biases.

4.4. Experiments

Experimental evaluation of IMU aided MAL with on-line inertial bias estimation, was carried out using an in-house built autonomous vehicle shown in Figure 4. The vehicle is equipped with an uncalibrated IMU (Crossbow DMU-AHRS), which is fixed to the vehicle frame as discussed in Section 4.2. A SICK LMS 290 range-bearing measurement sensor is used as the exteroceptive sensor. The sampling rates are 100 Hz and 10 Hz for the inertial sensor and the range-bearing sensor respectively. The speed of the vehicle was maintained at approximately 4 m/s. The centroid of a set of contiguous laser range points (cluster) at constant depth is chosen as a point feature. These clusters are formed from a laser scan using a simple clustering strategy based on the distance between contiguous and adjacent range points. The adjacent range points in a scan, which are within a certain distance threshold among each other, are clustered. If an adjacent range point is far from the current cluster, a new cluster is created. Now the centroid of each cluster is taken as the coordinates of the point feature or landmark. This simple distance based clustering is appropriate for range scans which give range and bearing values consecutively. It is observed in our experiments that the method of clustering can easily identify trees, lamp posts and other rigid objects in an outdoor setting.

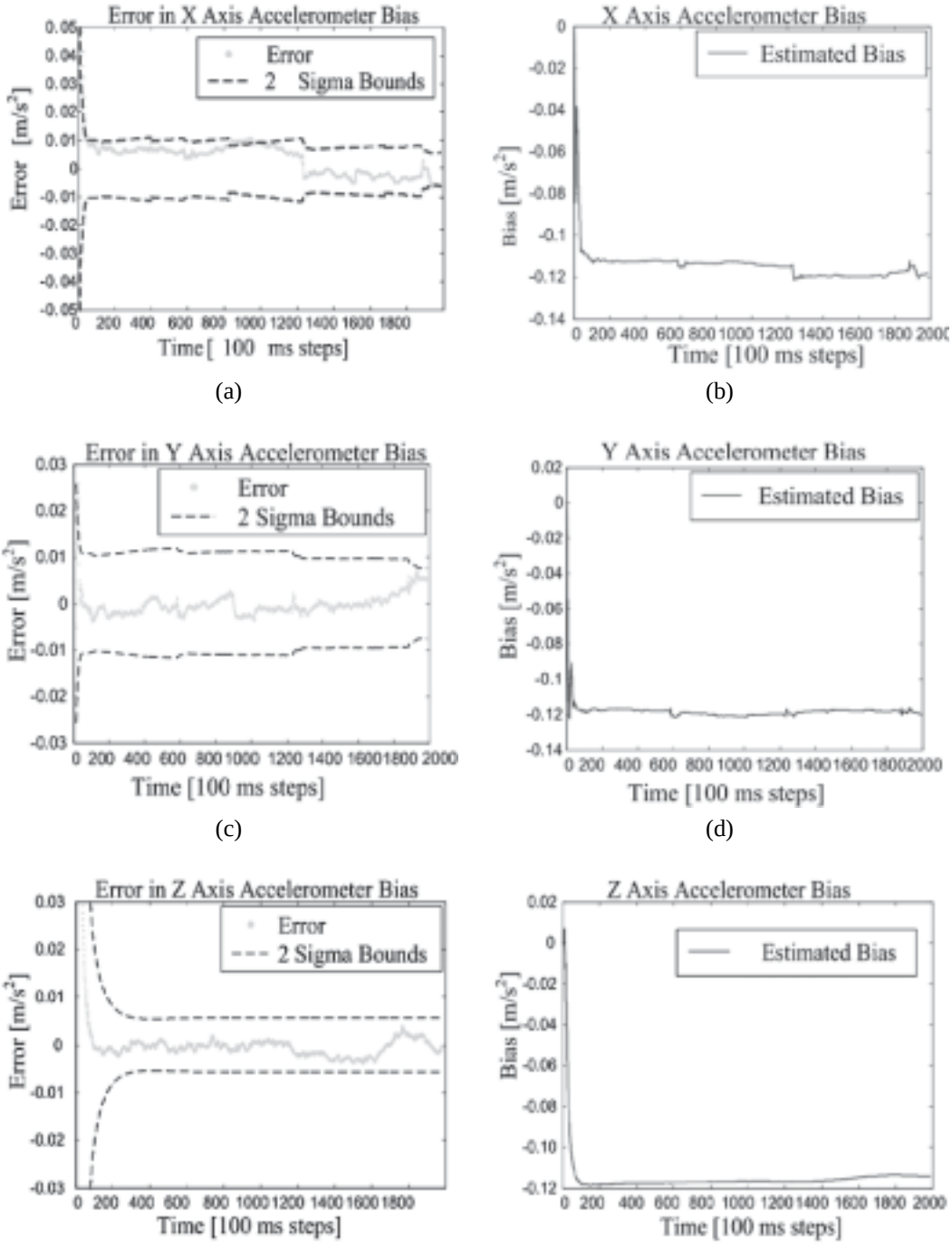

Fig. 8. Estimation of the accelerometer biases and their uncertainties in IMU aided MAL.

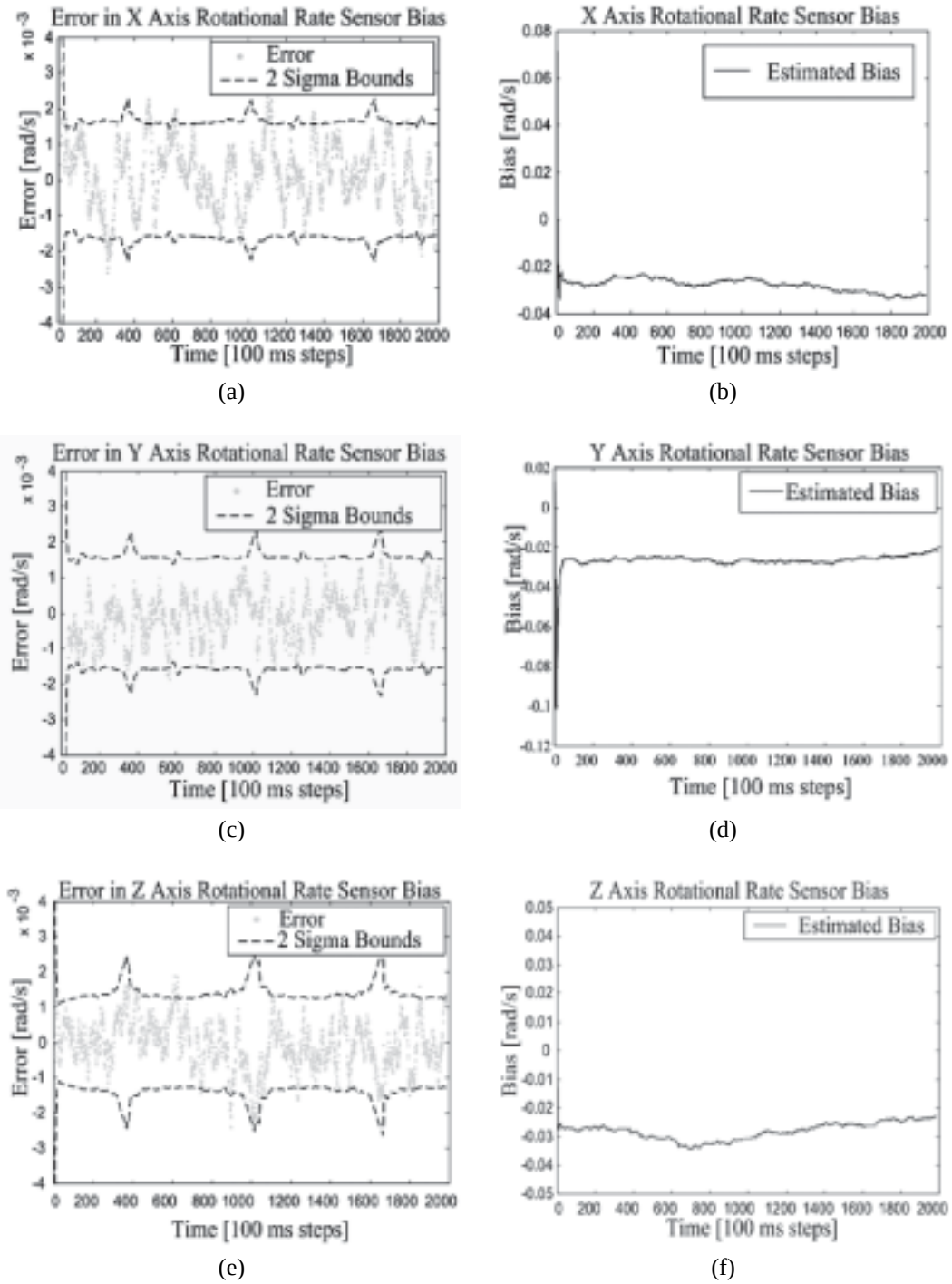

Fig. 9. Estimation of the gyro biases and their uncertainties in IMU aided MAL.

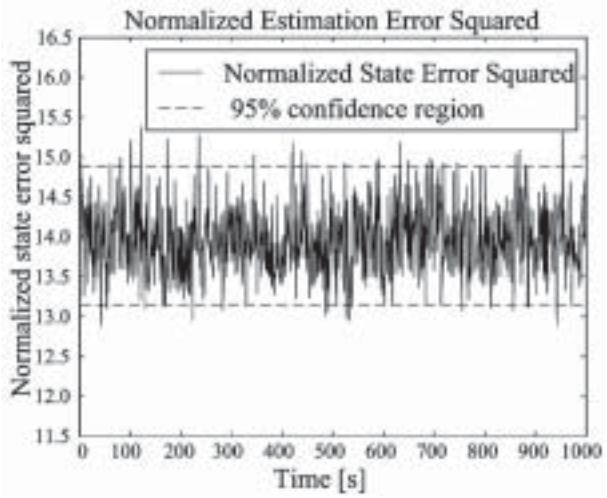

Fig. 10. The sample average values of the NEES for a 100 run Monte-Carlo simulation in IMU aided MAL. The 95% confidence regions are shown in dotted lines.

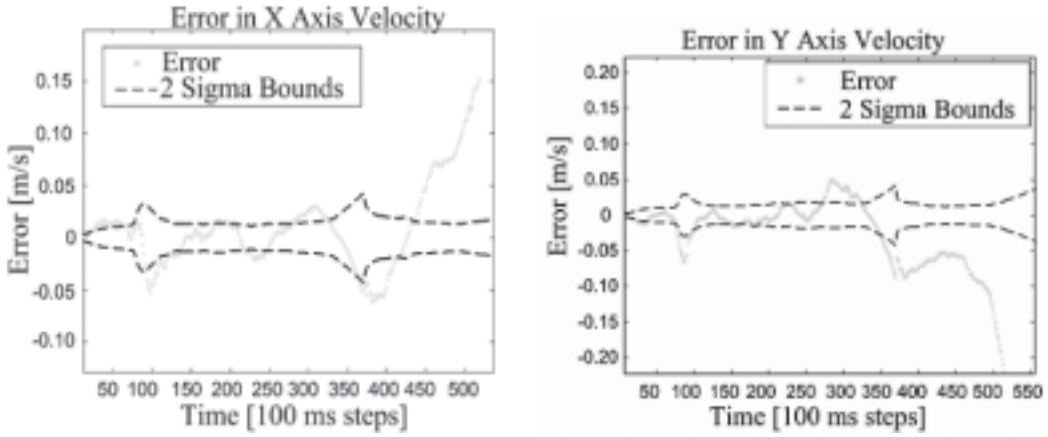

(a) (b)

Fig. 11. Velocity estimation errors in MAL with offline calibration.

Table 1. Rates of Divergence of the Algorithm

For constant rate sensor noise		For constant accelerometer noise	
Accelerometer Bias Random Walk ms/$\sqrt{\text{hr}}$	Time to Diverge (s)	Rate Sensor Bias Random Walk ($^0/\sqrt{\text{hr}}$)	Time to Diverge (s)
0.02	521	1	480
0.04	345	2	295
0.06	172	3	195
0.08	110	4	95
0.10	63	4.5	63

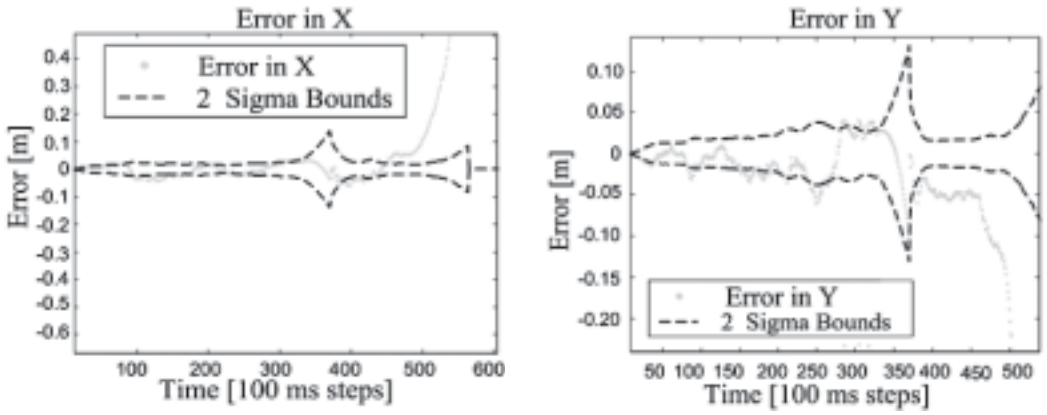

(a) (b)

Fig. 12. Location estimation errors in navigation frame in MAL with offline calibration.

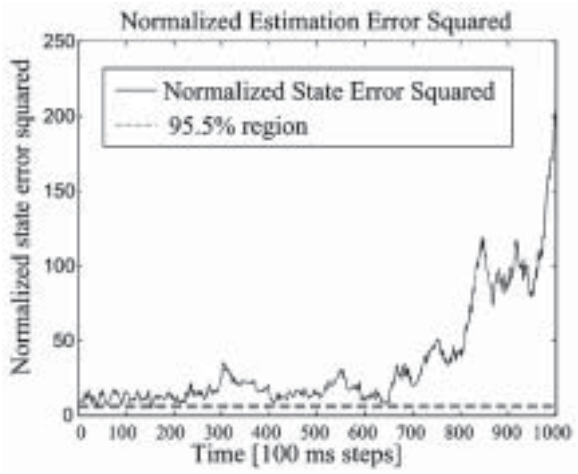

Fig. 13. Normalized state estimation squared error for 50 Monte-Carlo runs in IMU aided MAL with offline calibration. The 95% confidence regions are shown as dotted lines.

The experiment was conducted in a car park, where the surface is relatively flat and horizontal. The stored or a priori map is created manually by measuring the locations of a set of features, such as lamp posts and trees, in the area with respect to a predefined earth fixed navigation frame. The small circles in Figure 14 show the locations of the hand-measured features (true landmarks). The vehicle starting location is also measured by hand with reference to the navigation frame. The solid line in Figure 14 shows the estimated vehicle path when performing IMU aided MAL with online bias estimation. The crosses indicate landmarks observed and associated with the a priori map features (shown by the circles) when the vehicle is at the position indicated by the solid rectangle. The dotted line in Figure 14 represents the estimated vehicle path without online bias estimation. It is observed that there is a significant loop closing error with no online bias estimation in inertial aided MAL. Overall, it is clear from Figure 14 that without online bias estimation (correction) the location estimates are significantly erroneous.

The experimental results demonstrate that given sufficient number of landmark observations, the biases in the gyros and accelerometers can be jointly estimated with vehicle state online, without the aid of an absolute position sensor, such as GPS, which provides absolute information. These experimental results concur with the theoretical result governing full observability (Section 3.3) of inertial aided MAL with the online estimation of biases. The estimated acceleration and rate sensor biases and their 2σ bounds are shown in Figures 15, 16, 17 and 18 respectively. It is observed that uncertainties in biases diminish with updates over time and approach lower bounds, in agreement with the theory (Sections 3.1 and 3.2). The results also imply that observing enough landmarks which do not satisfy equations (70) and (71) is sufficient to make the otherwise unobservable IMU aided MAL with bias estimation observable. The initial constant components and the associated noise components of the inertial sensor biases are also estimated using offline methods described in Barshan and Durrant-Whyte (1995). As described in this work the data are obtained when the vehicle is stopped or stationary. It is estimated that on average the initial bias components of the accelerometers in the x, y and z axes directions are 0.075 ms^{-2}, 0.08 ms^{-2}, and 0.08 ms^{-2} respectively, and in the gyro 0.02 rad/s in all three axes directions. These results (Figures 14 to 18) are quite close to the values obtained in the MAL experiments involving online bias estimation.

5. Conclusions

In map aided localization the biases of proprioceptive and exteroceptive sensors can impair the viability of the estimation algorithm or compromise its performance. Standard brute

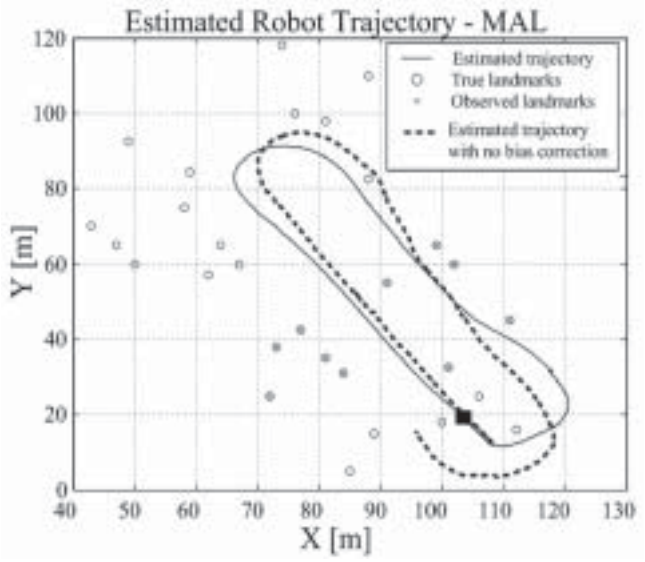

Fig. 14. IMU aided MAL with and without online bias estimation. The estimated paths with and without online bias estimation are shown by solid and dotted lines respectively. The vehicle at a particular instant is shown by the solid rectangle.

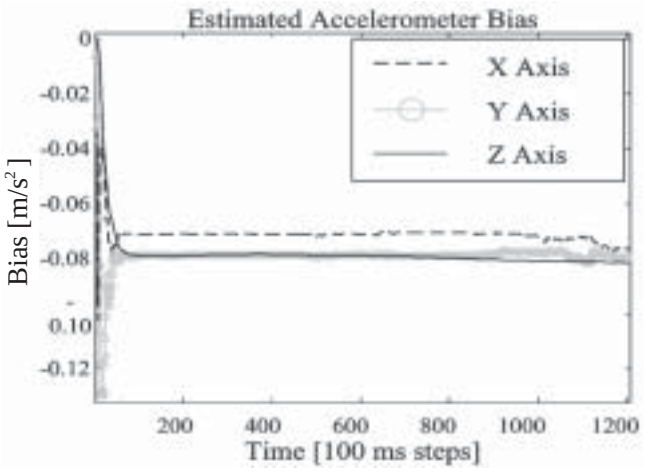

Fig. 15. Estimated accelerometer biases.

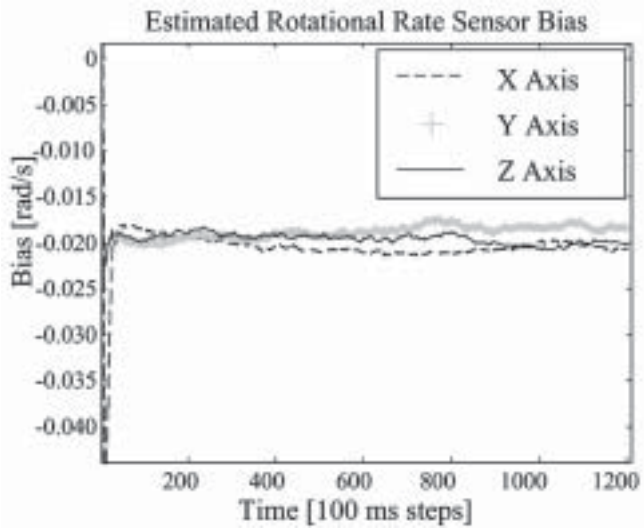

Fig. 16. Estimated rotational rate sensor biases.

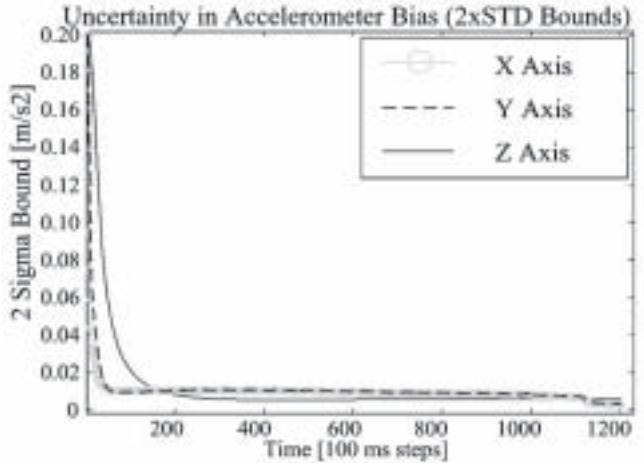

Fig. 17. Estimated 2σ uncertainty bounds of accelerometer biases.

force practices of calibrating or initializing sensors or estimating biases offline can in certain situations offset localization errors in MAL. However, these require longer setup times and periodic resetting of sensors rendering such techniques much less desirable in many practical applications, such as in autonomous navigation tasks. An effective and efficient methodology to alleviate problems in MAL due to sensor biases is to jointly estimate bias parameters of sensors with the vehicle state and apply corrections online. In this paper, such an approach was investigated in detail. The elaborate theoretical analysis, simulations and experimental results have provided valuable insight to the problem and established useful properties of the solution.

In the joint estimation of sensor biases in MAL, it is established that uncertainties of estimated errors in the bias parameters of both the proprioceptive and exteroceptive sensors diminish in each successive update and approaches a lower bound. This result is important in that it gives assurance that the accuracy of estimated biases improves at each update. As more and more measurement updates are incorporated, the bias parameters are determined with greater accuracy thereby guaranteeing accurate localization results regardless of the

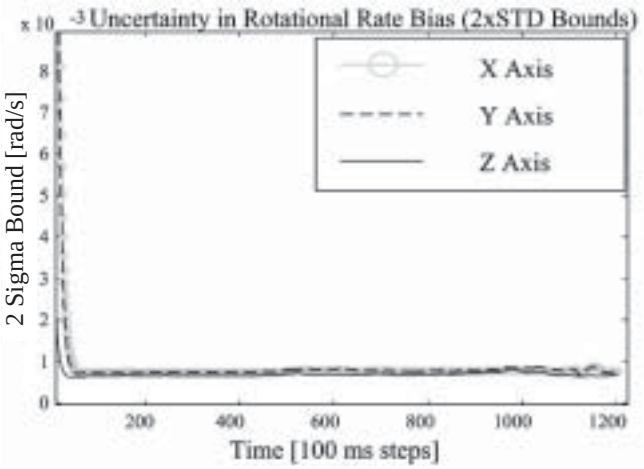

Fig. 18. Estimated 2σ uncertainty bounds of rotational rate sensor biases.

unknown biases in the sensors. The fact that the uncertainties of sensor biases have lower bounds enables us to estimate the bounds in localization accuracies, which is useful in any practical application of MAL.

Although often neglected in the literature on map aided localization, observability is a major issue when it comes to guaranteeing accurate localization. To ensure full observability in 2D, nonlinear MAL with online bias estimation, it is necessary to observe at least two landmarks, which are not simultaneously collinear with the vehicle position. In order to guarantee observability in IMU aided MAL with online bias estimation, it is necessary to observe at least two landmarks and simultaneously apply the nonholonomic constraints (virtual observations). It is important to note that observing two or more landmarks alone is not sufficient to ensure full observability. In all the above cases it was verified through simulations and experiments that satisfaction of the full observability conditions ensured consistent estimation of the bias parameters of the sensors and vehicle states, yielding accurate localization results. Moreover, given the a priori landmark map, these observability conditions enable a vehicle to plan its trajectory so as to guarantee the observability of the unknown bias parameters and thereby ensure correct vehicle localization.

The rate of convergence of the uncertainties, i.e., speed at which estimated quantities approach their true values, is also a vital indicator of algorithm performance, especially for real-time applications. For the linear 1D case, it is established that a smaller ratio between exteroceptive sensor noise and process noise (proprioceptive sensor noise and the modeling uncertainty) or a larger number of simultaneously observed landmarks, will result in faster convergence of the state variances to their steady state values. This result is helpful when selecting sensors based on their bias and noise characteristics and also the density of landmarks in the stored map. These observations about uncertainty variations are made even for nonlinear 2D models employed in standard MAL and INS aided MAL.

In conclusion, the theoretical findings and results substantiated by simulations and experiments provide greater insight into the problem of estimation theoretic bias correction in map aided localization. The investigations pave the way for the improved design and judicious choice of process and observation models and the selection of appropriate sensors for the enhanced performance of localization algorithms depending on the requirements of the mobile robot application.

Appendix

A matrix $\mathbf{A}_{nxn}$ is known to be PSD if $\underline{\mathbf{x}}^{\mathrm{T}}\mathbf{A}\underline{\mathbf{x}} \geqslant 0$, for all non zero $\underline{\mathbf{x}}_{nx1}$such that $\underline{\mathbf{x}} \in \mathbf{R}^n$.

Properties of the PSD Matrices

If $\mathbf{A}_{nxn}$ and $\mathbf{B}_{nxn}$ are PSD matrices, then:

1. $\mathbf{A} + \mathbf{B}$ is PSD
2. **AB** is PSD
3. Diagonal entries of **A** are nonnegative
4. $\det(\mathbf{A} + \mathbf{B}) \geqslant \det(\mathbf{A}) + \det(\mathbf{B})$
5. Any principal sub matrix of **A** is PSD

References

Bar-Shalom, Y. and Li, X. R. 2001. *Estimation with Applications to Tracking and Navigation: Theory Algorithms and Software*, John Wiley and Sons, Inc.

Barshan, B. and Durrant-Whyte, H. 1995. Inertial Navigation Systems for Mobile Robots. *IEEE Transactions on Robotics and Automation* 11(3):328–342.

Betke, M. and Gurvits, L. 1997. Mobile robot localization using landmarks. *IEEE Transactions on Robotics and Automation* 13(2):251–263.

Bingbing, L. and Adams, M. D. 2005. Multi Aided Inertial Navigation for Ground Vehicles in Outdoor Uneven Environments, *Proceedings of the IEEE International Conference on Robotics and Automation*, Barcelona, Spain.

Briechle, K. and Hanebeck, U. D.2004. Localization of a mobile robot using relative bearing measurements. *IEEE Transactions on Robotics and Automation* 20(1):36–44.

Brown, R. G. and Hwang, P. Y. C. 1992. *Introduction to Random Signals and Applied Kalman Filtering*, 2nd Edition, John Wiley and Sons Inc.

Durrant-Whyte, H. 2001. A Critical Review of the State-of-the-Art in Autonomous Land vehicle Systems and

Technology. *Sandia Report SAND2001-3685*, Albuquerque, New Mexico, Sandia National Laboratories.

Fang, J. C. and Wan, D. J. 1996. A Fast Initial Alignment Method for Strapdown Inertial Navigation System on Stationary Base. *IEEE Transactions on Aerospace and Electronic Systems* 32(4):1501–1505.

Fox, D., Burgard, W., Dellaert, F., and Thrun, S. 1999. Monte Carlo Localization: Efficient Position Estimation for Mobile Robots. *Proceedings of the 16th National Conference on Artificial Intelligence (AAAI 99)*, Orlando, Florida.

Friedland, B. 1969. Treatment of Bias in Recursive Filtering. *IEEE Transactions on Automatic Control* 14(4):359–367.

Grewal, M. G., Weill, L. R., and Andrews, A. P. 2001. *Global Positioning Systems, Inertial Navigation and Integration*. New York, John Wiley and Sons Inc.

Hicks, S. 1993. Advanced Cruise Missile Guidance System Description. *Proceedings of the IEEE 1993 National Aerospace and Electronics Conference (NEACON 1993)*, May 24–28.

Horn, R. A. and Johnson, C. R. 1985. *Matrix Analysis*, Cambridge University Press.

Hosteler, L. D. and Andreas, R. D. 1983. Nonlinear Kalman Filter Techniques for Terrain Aided Navigation. *IEEE Transactions on Automatic Control* 28(3):315–322.

Huster, A. and Rock, S. M. 2003. Relative Position Sensing by Monocular Vision and Inertial Rate Sensors. *IEEE International Conference on Robotics and Automation*, pp. 1562-1567.

Ignagni, M. 2000. Optimal and Suboptimal Separate Bias Kalman Estimators for a Stochastic Bias. *IEEE Transactions on Automatic Control* 45(3):547–551.

Kim, J. and Sukkarieh, S. 2004. Improving the Real-Time Efficiency of Inertial SLAM and Understanding its Observability, *IEEE International Conference on Intelligent Robots and Systems*, pp. 21–26.

Koifman, M. and Bar-Itzhack, Y. 1999. Inertial Navigation Systems Aided by Aircraft Dynamics, *IEEE Transactions on Control Systems Technology* 7:487–497.

Krishnan, V. and Grobert, K. 1970. Initial Alignment of a Gimballess Inertial Navigation Systems. *IEEE Transactions on Automatic Control* 15(6):667–671.

Leonard, J. J. and Durrant-Whyte, H. F. 1991. Mobile Robot Localization by Tracking Geometric Beacons. *IEEE Transactions on Robotics and Automation* 7(3):376–381.

Martinelli, A., Tomaties, N., Tapus, A., and Siegwart, R., 2003. Simultaneous Localization and Odometry Calibration for Mobile Robot, *Proceedings of the IEEE/RSJ International Conference on Intelligent Robots and Systems*, pp. 1499–1504.

Reif, K., Gunther, S., Yaz, E., and Unbehauen, R. 1999. Stochastic Stability of the Discrete–Time Extended Kalman Filter. *IEEE Transactions on Automatic Control* 44(4):714–278.

Roumeliotis, S. I., Sukhatme, G. S., and Bekey, G. A. 1999. Circumventing Dynamic Modeling: Evaluation of the Error-State Kalman Filter applied to Mobile Root Localization, *Proceedings of the IEEE International Conference on Robotics and Automation*, pp. 1656–1663.

Roy, N. and Thrun, S. 1999. Online Self-Calibration for Mobile Robots, *Proceedings of the IEEE International Conference on Robotics and Automation*, pp. 2292–2297.

Southall, B., Buxton B.F. and Marchant, J.A. 1998. Controllability and Observability: Tools for Kalman Filter Design. *Proceedings. of British Machine Vision Conference BMVC 1998*, Vol. 1, pp. 164–173.

Stronger, D. and Stone, P. 2005 Simultaneous Calibration of Action and Sensor Models on a Mobile Robot, *Proceedings of the IEEE International Conference on Robotics and Automation.*